1978

The Heating Of A Shock Tube Plasma With A Carbon-dioxide Laser

Stephen John Box

THE HEATING OF A SHOCK TUBE PLASMA WITH A CARBON DIOXIDE LASER

by

Stephen John Charles Box

Department of Physics

Submitted in partial fulfillment
of the requirements for the degree of
Doctor of Philosophy

Faculty of Graduate Studies
The University of Western Ontario
London, Ontario
May, 1978

ABSTRACT

The interaction of high-power pulsed lasers with plasmas has received much attention since the possibility of heating plasmas to thermonuclear temperatures was first suggested.

In this experiment, the absorption of CO_2 laser radiation by a plasma due to inverse bremsstrahlung was studied. The laser was shot into a plasma formed in an electromagnetic shock tube. The laser energy was approximately 0.3 J in a 180 ns pulse. The plasma had a density in the range from 10^{17} to $10^{18} cm^{-3}$ and a temperature of about 2eV. Spectroscopic methods were used to measure the plasma density and temperature both with and without laser irradiation. Direct observation of the path of the laser beam through the plasma was made using an image converter camera in conjunction with a narrow band interference filter. The propagation of the laser through the plasma and the energy absorption are discussed. The observed maximum increase in the electron temperature of the plasma due to the laser was 0.4eV.

Acknowledgements

The author wishes to express his sincere thanks to Dr. P.K. John for his guidance and encouragement throughout the course of this investigation.

He also wishes to thank Dr. E. Brannen and Dr. Z. Kucerovsky for helpful suggestions in building the laser, and to Dr. E.A. McLean for informative discussions on plasma spectroscopy.

Special thanks are extended to Dr. W.W. Byszewski for useful discussions.

To my wife Dale

TABLE OF CONTENTS

LIST OF FIGURES

LIST OF TABLES

CHAPTER 1: INTRODUCTION

1.1 General Introduction

The problem of controlled thermonuclear fusion has provided much of the impetus to the study of plasma physics, since the achievement of a controlled thermonuclear reaction would provide a virtually unlimited supply of energy. In thermonuclear fusion reactions the nuclei of light elements combine to form heavier nuclei and results in the release of large amounts of nuclear energy. Since nuclei are positively charged, they repel one another. Therefore in order for the fusion reactions to occur the nuclei must have kinetic energies large enough to overcome the Coulomb barrier between them. The reacting elements must therefore be heated to a high temperature and confined for a time long enough for the thermonuclear reactions to occur.

In the case of deuterium and tritium the temperature must be ~4keV before the energy gained from the fusion reactions exceeds the loses due to bremsstrahlung radiation by the electrons. This temperature is called the ignition or breakeven temperature. For the fusion of deuterium alone a temperature of ~35keV is required. These high temperatures are the reason why fusion research involves plasma physics since at these temperatures all matter is in the plasma state.

The problems involved in achieving a fusion reactor can be divided into three categories:

1. Plasma heating
2. Plasma confinement
3. Fusion technology

This work will only be concerned with the first category, namely plasma heating.

Heating of plasmas can be accomplished by a number of methods [1] some of which are listed below.

1. Ohmic heating. This is the heating of a plasma by the passage of a current through it.
2. Adiabatic compression.
3. Beam-plasma interaction.
4. Magnetic pumping.
5. Shock heating.
6. Laser heating.

The last mentioned method, laser heating is the subject of this work.

Some of the first theoretical bases of laser heating of plasmas were investigated by Dawson et al [2,3] and independently by Basov [4]. As a laser beam propagates through a plasma it is absorbed resulting in an increase in the plasma temperature.

At very high laser light intensities the laser can cause instabilities in the plasma which can result in enhanced absorption of the laser radiation [5,6]. However high densities are required for these effects and thus if the plasma is being confined magnetically as most fusion plasmas are, then the magnetic fields required are far beyond our present

technology.

At lower intensities the laser light is absorbed by classical inverse bremsstrahlung, which is the resistive damping of the light wave due to electron-ion collisions. This process is linear in the laser intensity.

The absorption coefficient for inverse bremsstrahlung is given by [7,8]

$$\alpha = 4.4 \times 10^{-37} n_e^{\,2} \lambda^2 T_e^{\,-3/2} cm^{-1}. \qquad (1\text{-}1)$$

where n_e is the electron density in cm^{-3}, λ is the laser wavelength in microns and T_e is the electron temperature in eV.

Two of the lasers which are currently being investigated with regard to laser heating are the neodymium glass laser, emitting 1 micron radiation and the carbon dioxide laser which emits 10.6 micron radiation. Examination of equation (1-1) indicates one of the advantages of the carbon dioxide laser. The absorption coefficient depends on λ^2 so longer wavelengths are absorbed in a much shorter length in the plasma. In addition carbon dioxide lasers of high power and high quantum efficiency have been built. Energy output of ~10kJ per pulse have been achieved. The quantum efficiency of a carbon dioxide laser is 40% and efficiencies of about 25% have been obtained in practice.

Since the absorption coefficient also depends on $n_e^{\,2}$, it is desirable to have a large density in order to have the laser light absorbed in a reasonable plasma length. However an upper limit is also set by the requirement of magnetic confinement. The magnetic field necessary to confine the plasma increases as $\sqrt{n_e}$ so n_e is limited by our

ability to produce large magnetic fields. In the particular case of CO_2 laser radiation the density cannot be greater than $10^{19} cm^{-3}$ in any event since for densities above this critical density the laser radiation is reflected at the plasma boundary. For reasonable plasma lengths, the CO_2 laser can effectively heat plasmas in the density range $10^{17} cm^{-3}$ to $10^{19} cm^{-3}$.

It should also be noted from equation (1-1) that the absorption coefficient decreases as the three halves power of T_e, so that as the temperature of the plasma increases the laser becomes less efficient at heating it. Since for fusion purposes it is not desirable to keep T_e small fusion plasmas will likely have to be rather long and as dense as possible.

In summary it is the long wavelength, high power and high efficiency which make the CO_2 laser attractive for fusion experiments.

The first results obtained in laser-plasma heating were reported by Engelhardt et al [9]. Since then a number of authors have reported work on laser heating of plasmas with varying degrees of success [10,11, 12,13,14,15].

CHAPTER 2

A: THEORY OF ABSORPTION OF LASER RADIATION BY A PLASMA

2.1 Introduction

The theory of laser beam absorption can be divided into two main sections. The theory of classical inverse bremsstrahlung absorption will be discussed in detail in section 2.2. Most of the experimental work performed to date has involved inverse bremsstrahlung and it is this type of absorption which applies directly to the experiments described in this work. All absorption mechanisms not involving classical inverse bremsstrahlung are referred to as anomalous absorption. Anomalous absorption plays a particularly important role in laser-pellet fusion experiments but is not as important in laser-plasma fusion. Some aspects of anomalous absorption will be briefly discussed in section 2.3.

2.2 Calculation of the Inverse Bremsstrahlung Absorption Coefficient for a Plasma

When electromagnetic radiation enters a plasma it causes the electrons to accelerate. The electrons collide with the ions in the plasma which randomizes the electron motion resulting in the energy of the

wave being inverted into thermal energy of the electrons. We start with Maxwell's equations, in MKS units.

$$\bar{\nabla}\cdot\bar{E} = \rho/\varepsilon_0 \tag{2-1}$$

$$\bar{\nabla}\cdot\bar{B} = 0 \tag{2-2}$$

$$\bar{\nabla}\times\bar{E} = -\frac{\partial\bar{B}}{\partial t} \tag{2-3}$$

$$\bar{\nabla}\times\bar{B} = \frac{1}{c^2}\frac{\partial\bar{E}}{\partial t} + \mu_0\bar{J} \tag{2-4}$$

We can also write Langevin's equation for a plasma

$$m\frac{d\bar{u}}{dt} = -e[\bar{E}+\bar{u}\times\bar{B}] - m\nu_c\bar{u} \tag{2-5}$$

where $\bar{u}$ is the average velocity for the electrons, m is the electron mass and ν_c is the average number of collisions per second which an electron has with the ions in the plasma.

Solutions to equations (2-1) to (2-5) are sought which have the following form

$$\begin{pmatrix} \bar{E}(x,t) \\ \bar{B}(x,t) \\ \bar{u}(x,t) \end{pmatrix} = \begin{pmatrix} \bar{E} \\ \bar{B} \\ \bar{u} \end{pmatrix} e^{i(kx-\omega t)} \tag{2-6}$$

where k is the propagation constant for a wave travelling in the x-direction, and ω is the angular frequency.

In Langevin's equation (2-5) it is generally possible to neglect the $\bar{u}x\bar{B}$ term since it is usually much less than the $\bar{E}$ term. Since $B = \frac{\bar{k}x\bar{E}}{\omega}$, the magnitude of the $\bar{u}x\bar{B}$ term is always less than $|\frac{ukE}{\omega}|$ whereas the $\bar{E}$ term has the magnitude $|E|$. Therefore $\bar{u}x\bar{B}$ can be neglected provided $|u|<<|\omega/k|$. Usually, ω/k, the phase velocity is of the order of c whereas $\bar{u}$ is much smaller.

By substituting equation (2-6) into equations (2-1) to (2-5) the following equation can be derived.

$$\bar{\nabla}x(\bar{\nabla}x\bar{E}) = [\frac{\omega^2}{c^2} - \frac{\omega\omega_p^{\ 2}}{c^2(\omega+i\nu_c)}]\bar{E} \qquad (2-7)$$

where $\omega_p^{\ 2} = \frac{n_e e^2}{m\varepsilon_0}$.

ω_p is the plasma frequency and may be thought of as the frequency at which the electrons oscillate about their equilibrium positions.

Replacing $\bar{\nabla}$ by $i\bar{k}$ equation (2-7) becomes

$$-\bar{k}x(\bar{k}x\bar{E}) = -\bar{k}(\bar{k}\cdot\bar{E}) + k^2\bar{E} = +[\frac{\omega^2}{c^2} - \frac{\omega\omega_p^{\ 2}}{c^2(\omega+i\nu_c)}]\bar{E} \qquad (2-8)$$

For longitudinal waves $\bar{k}x\bar{E} = 0$ so from equation (2-8) one obtains

$$\omega^2 = \frac{\omega_p^{\ 2}}{1+i\nu_c/\omega}$$

or $$\omega = \frac{-i\nu_c \pm \sqrt{4\omega_p^{\ 2} - \nu_c^{\ 2}}}{2}$$

For all values of ν, ω has a negative imaginary part, so the waves, which are proportional to $e^{-i\omega t}$ are damped.

For transverse waves $\bar{k}\cdot\bar{E} = 0$ and equation (2-8) leads to the following dispersion relation

$$k^2c^2 - \omega^2 + \frac{\omega\omega_p^2}{(\omega+i\nu_c)} = 0$$

By defining the electron-ion collision time, $\tau_c = 1/\nu_c$, we have

$$k^2c^2 - \omega^2 + \frac{\omega\omega_p^2}{\omega+i/\tau_c} = 0 \qquad (2\text{-}9)$$

Generally $\nu_c \ll \omega$ so (2-9) can be approximated by

$$k^2c^2 - \omega^2 + \omega_p^2(1 - \frac{i}{\omega\tau_c}) = 0 \qquad (2\text{-}10)$$

Solving equation (2-10) for k gives

$$k = \pm \frac{\sqrt{\omega^2-\omega_p^2}}{c} \pm \frac{i\,\omega_p^2}{2c\omega(\omega^2-\omega_p^2)^{1/2}\tau_c} \qquad (2\text{-}11)$$

The intensity of the electromagnetic wave falls off spatially as $e^{-\alpha x}$ where the absorption coefficient α can be obtained from equation (2-11)

$$\alpha = \frac{\omega_p^2}{c\omega\tau_c(\omega^2-\omega_p^2)^{1/2}} \qquad (2\text{-}12)$$

τ_c, the electron-ion collision time is given by [16]

$$\tau_c = \frac{3}{2\pi}^{3/2} \frac{(KT_e)^{3/2}m^{1/2}}{Z^2e^4n_i} \ln\left(\frac{\lambda_D}{r_{min}} \frac{\nu_p}{(\nu^2+\nu_p^2)^{1/2}}\right) \qquad (2\text{-}13)$$

where $\lambda_D = \frac{\varepsilon_0 KT}{n_e e^2}$ is the Debye length and r_{min} is the minimum impact parameter. For r_{min} one chooses the larger of the inverse de Broglie wavelength $(\frac{\hbar}{\sqrt{mKT_e}})$ or the classical distance of closest approach $(\frac{KT}{Ze^2})$. The dependence of τ_c on ν is small and is usually neglected.

Substituting equation (2-13) into equation (2-12) gives the following expression for the absorption coefficient [8]

$$\alpha = \frac{16\pi Z^2 n_e n_i e^6 \ln\Lambda(\nu)}{3c\nu^2(2\pi m_e KT)^{3/2}(1-\nu_p^2/\nu^2)^{1/2}} \qquad (2\text{-}14)$$

where $$\Lambda = \frac{\lambda_D}{r_{min}} \frac{\nu_p}{(\nu_p^2+\nu^2)^{1/2}}$$

Finally the numerical formula for the absorption coefficient with $n_i = Zn_e$ and $Z = 1$ is

$$\alpha = 4.4 \times 10^{-37} n_e^2 \lambda^2 T_e^{-3/2} cm^{-1} \qquad (2\text{-}15)$$

where n_e is in cm^{-3}

λ_D is in microns

T_e is in electron volts

The factor $(1 - \frac{\nu_p^2}{\nu^2})^{1/2}$ is important only when $\nu_p \approx \nu$ and is neglected.

$$\Lambda = \frac{1.23 \times 10^7 T_e^{3/2}}{n_e^{1/2}} \text{ [17]}$$

Another useful concept is that of absorption length ℓ. The absorption length ℓ is defined as the distance in the plasma at which the laser intensity falls to 1/e of its initial intensity. Therefore $\ell = 1/\alpha$ cm or

$$\ell = \frac{2.3\times10^{36}T_e^{3/2}}{n_e^2\lambda^2} \qquad (2\text{-}16)$$

2.3 Anomalous Heating of a Plasma

If the intensity of the laser is sufficiently intense, it can drive low frequency instabilities in the plasma which amplify fluctuations in the plasma to produce large amplitude ion waves. These waves can cause a large increase in the high frequency resistivity of the plasma resulting in much shorter absorption lengths for the laser and consequently increased heating.

Ginsburg [18] and Hora [19] have shown that if a laser is incident on a plasma at an angle to the density gradient of the plasma and if the electric vector of the incident laser is in the plane of incidence then part of the electromagnetic energy is transformed into electrostatic energy of plasma waves. These plasma waves are then damped by Landau damping thus heating the plasma.

Another type of anomalous absorption is due to the large increase in resistivity of the plasma when $\omega\sim\omega_p$. The increased resistivity arises because ion density fluctuations can couple the electromagnetic wave to longitudinal plasma oscillations. Strong ion density fluctuations are necessary to make the resistivity increase significantly and these strong fluctuations can be caused by the laser itself since it can

cause instabilities in the plasma. One such instability is the thermal instability first suggested by Kidder and reported by Dawson [20]. Ion acoustic waves become unstable when energy is fed into a certain volume at a rate faster than it can be diffused away.

Another type of instability investigated by Dubois and Goldman [21], occurs when energy is fed into plasma oscillations faster than it can be dissipated away. If the plasma frequency ω_p is close to the incident laser frequency, ω, then the two frequencies can beat together and pump the plasma at the low frequency ω_i when $\omega_i = \omega - \omega_p$ (ω_i is the frequency characteristic of the ion acoustic waves). Also ω and ω_i can beat together and pump the plasma at ω_p. Thus the plasma can become unstable at ω_p and ω_i. This instability is of the type known as parametric instabilities. Another parametric instability occurs when $\omega \approx 2\omega_p$ [22].

Various anomalous heating mechanisms are discussed by Kaw and Dawson [20] along with the laser power thresholds required to produce them. No anomalous absorption is expected for the low power used in this experiment.

B: SPECTROSCOPIC DETERMINATION OF ELECTRON DENSITY AND TEMPERATURE

2.4 Density Calculations

The electron density in the plasma was measured using Stark broadening of either or both of the HeI line at 5876 Å and the HeII line at 4686 Å.

The profiles of lines emitted by atoms or ions are determined predominantly, at high densities, by the interaction of the emitters with the surrounding particles. The interaction results in the lines being broadened and is referred to as pressure broadening. There are three types of pressure broadening. They are resonance broadening, Van der Waals broadening and Stark broadening. Only Stark broadening is discussed here since it is the main broadening mechanism when ionization exceeds 1%.

There is one general theory of Stark broadening of which there are two extremes; the impact theory and the quasi-static theory.

The impact theory assumes the emitting particle is subject to a series of fast impacts. The wavetrain of light emitted by the particle is broken up into a number of smaller wavetrains. A Fourier analysis of these short wavetrains and statistical averaging over times between collisions gives the intensity distribution of the line. It is usually

Lorentzian in shape.

In the quasi-static theory the particle is considered to be continuously under the influence of perturbers during the entire emitting process. The perturbing particles are considered to be moving slowly.

The impact theory is used for electron broadening calculations and the quasi-static theory is used for ion broadening. Both broadening theories are combined in the complete theory.

Shown in Table 2-1 taken from Griem [33] are the calculated Stark broadening parameters for the HeI line at 5876 Å. ω is the electron impact half half width; d/ω is the relative electron impact shift and α is the ion broadening parameter. The widths ω are in Angstroms and their exponents indicate the power of ten by which the entries must be multiplied to obtain the electron impact half half widths at an electron density $n_e' = 10^{16} cm^{-3}$. They are converted to other densities n_e by multiplying by n_e/n_e'. The ion broadening parameters α, are converted to other densities by multiplying by $(n_e/n_e')^{1/4}$. d/ω is relatively independent of the density. Using the values from Table 2-1 the total half half width can be calculated using the following formulae.

$$\omega_{total} = 1 + 1.75\alpha(1-0.75r)\omega \qquad (2\text{-}17)$$

$$d_{total} = d/\omega \pm 2.0\alpha(1.0-0.75r)\omega \qquad (2\text{-}18)$$

where $$r = \frac{\text{mean distance between ions}}{\text{Debye length}} \qquad (2\text{-}19)$$

Table 2-1: Stark broadening parameters for the HeI line at 5876 Å

WAVELENGTH	T (°K)	2500	5000	10000	20000	40000	80000
5876 Å	ω	1.62 $^{-1}$	1.80 $^{-1}$	186 $^{-1}$	1.86 $^{-1}$	1.82 $^{-1}$	1.72 $^{-1}$
	d/ω	-0.845	-0.577	-0.336	-0.124	0.043	0.143
	$\alpha\zeta$	0.064	0.059	0.058	0.058	0.059	0.061

The above formulae are for neutral emitters. For singly ionized emitters the .75r terms must be replaced by 1.2r.

Griem [33] also gives what are known as reduced Stark profiles, $S(\alpha)$, for hydrogen, ionized helium and hydrogenic neutral He lines. α is a reduced wavelength distance given by $\alpha = \Delta\lambda/F_o$ where $\Delta\lambda$ is the distance from the line center (in $\mathring{A}$) and F_o, the Holtzmark field strength, is given by

$$F_o = 1.25 \times 10^{-9} n_e^{2/3} \qquad (2\text{-}20)$$

F_o is an average electric field in the plasma.

The tabulated profiles are normalized so that

$$\int_{-\infty}^{\infty} S(\alpha)d\alpha = 1 \qquad (2\text{-}21)$$

Table 2-2 is taken from Griem [33]. It gives the tabulated Stark profiles for the HeII line at 4686 $\mathring{A}$. The most accurate way of determining the density is to use the table to plot the Stark broadened profiles of the line for various combinations of temperature and density and see which graph fits the experimental data the best.

A simpler method that works well is to use the formula for the half width $\Delta\lambda_{1/2}$ of the profile given below.

$$\Delta\lambda_{1/2} = 2.5 \times 10^{-9} \alpha_{1/2} n_e^{2/3} \mathring{A} \qquad (2\text{-}22)$$

As an example suppose we wish to find the width of the HeII line at 4686 $\mathring{A}$ at an electron temperature of 40000 K and a density of

Table 2-2: Reduced Stark profiles for the HeII line at 4686 Å

HeII 4,686 Å														
T, °K	N, cm^{-3}	$\alpha = 0.000$	0.002	0.004	0.007	0.010	0.015	0.020	0.030	0.040	0.050	0.070	0.100	0.140
0.5×10^4	10^{14}	53.4	48 0	37.6	24.4	17.0	10.0	6.36	2.98	1.69	1.04	0.46	0.19	0.08
1×10^4	10^{13}	58.6	47.8	33.6	21.0	14.7	9.00	6.14	2.96	1.65	1.00	0.47	0.20	0.08
	10^{14}	45.1	41.3	34 4	25.0	17.9	11.0	7.42	3.93	2.36	1.50	0.72	0.30	0.13
2×10^4	10^{13}	63.1	48.5	32.9	20.3	14.7	9.54	6.70	3 42	1.95	1.19	0.54	0.20	0.08
	10^{14}	48.0	38.3	27.5	19.2	14.4	9.63	6.89	3.65	2.18	1.36	0.64	0.27	0.12
	10^{15}	36.8	33.1	26.8	19 2	14.7	9.60	6.66	3.44	2.05	1.32	0.66	0.30	0.14
4×10^4	10^{13}	68.9	49.5	29.5	18.1	12.8	7.96	5.48	2.86	1.64	1.01	0 46	0.18	0.08
	10^{14}	49.5	36.8	25.9	18.6	14.1	9.53	6.86	3.61	2.08	1.30	0.60	0.24	0.10
	10^{15}	38.0	34.4	27.2	18.9	14.4	9.69	7.02	3.79	2.20	1.38	0.64	0.29	0.13
	10^{16}	31.0	28.9	24.8	18.3	13.8	9.35	6.46	3.32	2.13	1.38	0.68	0.32	0.15
	10^{17}	23.9	23.3	21.5	17.5	14.0	9.23	6 16	3.49	2.13	1.41	0.72	0 34	0.18
8×10^4	10^{15}	41.9	38.1	27.6	19.2	14.0	9.22	6.41	3.36	1.96	1.22	0.56	0.24	0.11
	10^{16}	29.5	27.5	23.7	17.4	14.1	10.0	7.19	4.12	2,53	1.69	0.85	0 40	0.18
	10^{17}	25.1	24.2	21.6	17.0	13.6	9.90	7.32	4.22	2.62	1.76	0.92	0.44	0.22

Table 2-3: Values of the function $C(n_e,T_e)$ as a function of n_e and T_e for the line HeII (4686 Å)

n_e (cm^{-3})

T (K)	10^{15}	10^{16}	10^{17}	10^{18}	10^{19}
5000	1.58×10^{16}				
10000	2.41×10^{16}	1.09×10^{16}			
20000	2.86×10^{16}	2.30×10^{16}	1.24×10^{16}		
40000	4.34×10^{16}	2.74×10^{16}	1.37×10^{16}	9.87×10^{15}	6.24×10^{15}
80000			1.65×10^{16}	9.07×10^{15}	6.74×10^{15}

$1.0 \times 10^{17}cm^{-3}$. From Table 2-2 we see that $S(\alpha) = 38$ at $\alpha = 0$. $\alpha_{\frac{1}{2}}$ is the value of α at which $S(\alpha)$ is half its maximum value. Therefore from the table we find the value of α which gives $S(\alpha) = 19$. This gives $\alpha_{\frac{1}{2}} = .007$. Therefore the half width is

$$\Delta\lambda_{\frac{1}{2}} = 2.5 \times 10^{-9} \times .007 \times (10^{17})^{2/3}$$

$$= 3.8 \text{ Å}$$

Another method of finding the density is to use a table such as Table 2-3 also taken from Griem [33]. The table gives values of a function $C(n_e,T_e)$ for various temperatures and densities. From these values of C, the electron density can be calculated using the following formula.

$$n_e = C(n_e,T_e)\Delta\lambda_{\frac{1}{2}}^{3/2} cm^{-3} \qquad (2\text{-}23)$$

As an example suppose the temperature is 40000 K and the density is approximately $10^{17}cm^{-3}$. From the table $C = 1.37 \times 10^{16}$. If the experimental half width is 3.8 Å then equation (2-23) gives $n_e = 1.0 \times 10^{17}cm^{-3}$.

If we had estimated the density to be $10^{16}cm^{-3}$ then from the table $C = 2.74 \times 10^{16}$. Equation (2-23) gives the density $n_e = 2.0 \times 10^{17}cm^{-3}$ so we would have known that the estimate of $10^{16}cm^{-3}$ was incorrect.

It should be mentioned that Stark broadening is not the only broadening mechanism in a plasma. Lines can be broadened due to

Doppler broadening and natural broadening. However natural broadening is usually less than 10^{-4}Å and so is negligible in our experiment. Doppler broadening is largest for light elements at high temperatures. For low energy plasmas (ie. T_e<10eV) the electron density must be less than ~10^{15} cm^{-3} in order for the Doppler broadening to predominate over Stark broadening.

2.5 Temperature Calculations

If LTE is assumed then temperature measurements can be made by measuring relative line intensities. In principle this could be accomplished by measuring the relative line intensities of lines from the same ionization stage, however the intensity ratio is a function of the difference in excitation energy of the upper level of the lines and since the upper level of the lines are usually close in energy the intensity ratio is only a weak function of the temperature. This situation is greatly improved if lines from successive ionization stages of the same element are used because now the effective energy difference is enhanced by the ionization energy. The ratio of the densities of atoms or ions of the same species and stage of ionization in states with energies E_n and E_m is given by [33]

$$\frac{n_n}{n_n} = \frac{g_n}{g_m} \frac{\exp(-E_n/kT)}{\exp(-E_m/kT)} \qquad (2\text{-}24)$$

The numerator and denominator are the Boltzmann factors associated with the energy levels E_n and E_m. For most levels the statistical weights, g, are given by the number of orientations that the total

angular momentum can assume.

$$g = 2J+1$$

The Saha equation can be written as

$$\frac{n_e n_1^{\,z}}{n_n^{\,z-1}} = \frac{2g_1^{\,z}}{g_n^{\,z-1}}\left(\frac{mT_e}{2\pi\hbar^2}\right)^{3/2}\exp\left(-\frac{E_n'}{T_e}\right) \qquad (2\text{-}25)$$

where z is the effective charge acting on the radiating electron

n^{1z} is the density of ions in the ground state and E_n' is the ionization energy from level n except for a correction accounting for Coulomb interactions in dense plasmas and $n_n^{\,z-1}$ is the density of ions in state n. Let $I(\omega,\Theta,b)$ be the electromagnetic radiation leaving the plasma at a point x=b ie. the power per unit area, solid angle and angular frequency interval. If x=a is the opposite boundry of the plasma and $\gamma(\omega,x)$ is the optical depth measured back into the plasma from the point x=b then

$$\lim_{\gamma_a \to 0} \int I(\omega,\Theta,a)d\omega = \frac{h\omega^3 r_o}{2\pi c}\frac{g_n}{g_m} f_{mn} \int_a^b N_m(x)dx \qquad (2\text{-}26)$$

where f_{mn} is the absorption oscillator strength and $N_m(x)$ is the density of atoms in state m.

From equations (2-24), (2-25) and (2-26) it can be shown that [33]

$$\frac{I'}{I} = \frac{f'g'\lambda'^3}{fg\lambda^3}(4\pi^3/^2 a_o^3 n_e)^{-1} \left(\frac{T_e}{13.6}\right)^{3/2} \exp\left(\frac{E'+E_\infty-E-\Delta E_\infty}{T_e}\right) \qquad (2\text{-}27)$$

Primed quantities refer to the line from the higher ionization stage and ΔE_∞ is the reduction of the ionization energy E_∞ of the lower ionization stage.

$$\Delta E_\infty^{\,z-1} = \frac{Ze^2}{4\pi\varepsilon_0\lambda_D} \qquad (2\text{-}28)$$

z = 1 for neutrals, 2 for singly ionized etc.

a_o is the Bohr radius

f is the absorption oscillator strength

E is the excitation energy of the upper level of the line

λ_D is the Debye length.

CHAPTER 3: EXPERIMENTAL APPARATUS

3.1 The Carbon Dioxide Laser

For the reasons pointed out in the introduction the laser chosen for this heating experiment was the carbon dioxide laser. In order to heat a plasma it is desirable to have large laser power so it was necessary to use a pulsed high pressure laser. The laser medium, to be discussed later, was pumped using an electrical discharge transverse to the laser axis. Such TEA lasers (transverse electric field atmospheric pressure) were first reported by Beaulieu [23].

A schematic diagram of the laser is shown in Figure 3-1. The laser tube was a 3.5 m long acrylic tube of inside diameter 1.75". The tube was sealed at each end with a sodium chloride flat of diameter 50 mm and thickness 5 mm set at the Brewster angle.

The cavity mirrors were both made of germanium and were supplied by Oriel Optics. The mirrors were concave spherical mirrors of diameter 1.5 inches. One side of each mirror was flat, while the concave side had a radius of curvature of 10 m. One mirror was coated on the concave side to have a reflectivity of 99.8%. The output mirror was antireflection coated on the flat side and coated to provide a reflectivity of 65% on the concave side. The cavity length was 4 m,

Figure 3-1: Schematic of the carbon dioxide laser

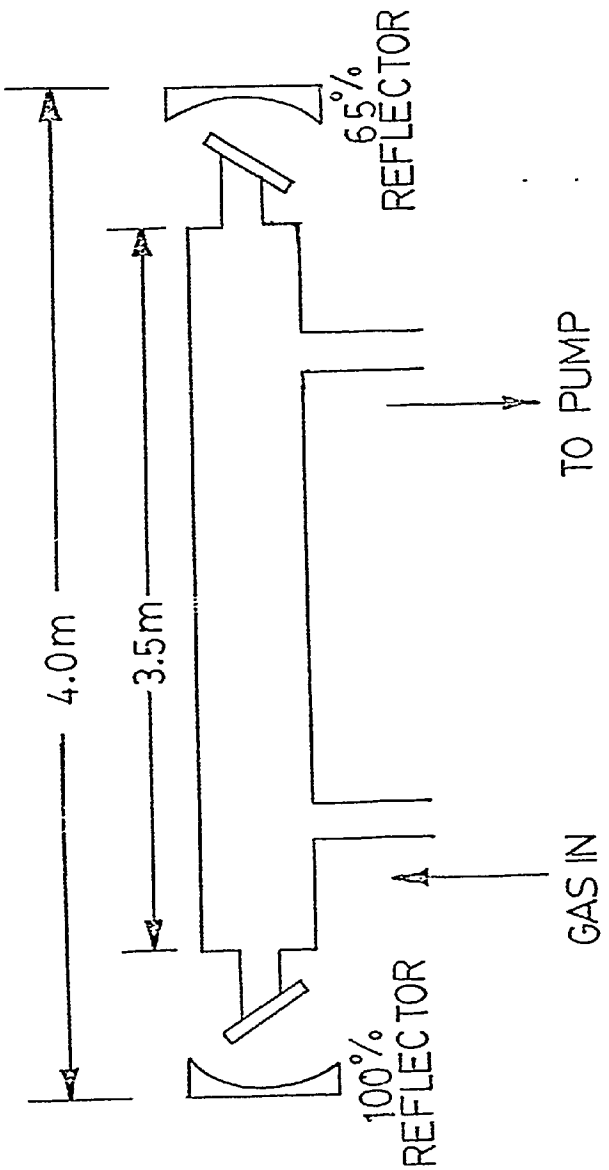
65%
REFLECTOR
TO PUMP
4.0m
3.5m
GAS IN
100%
REFLECTOR

Figure 3-2: Photograph of a section of the helical laser electrodes

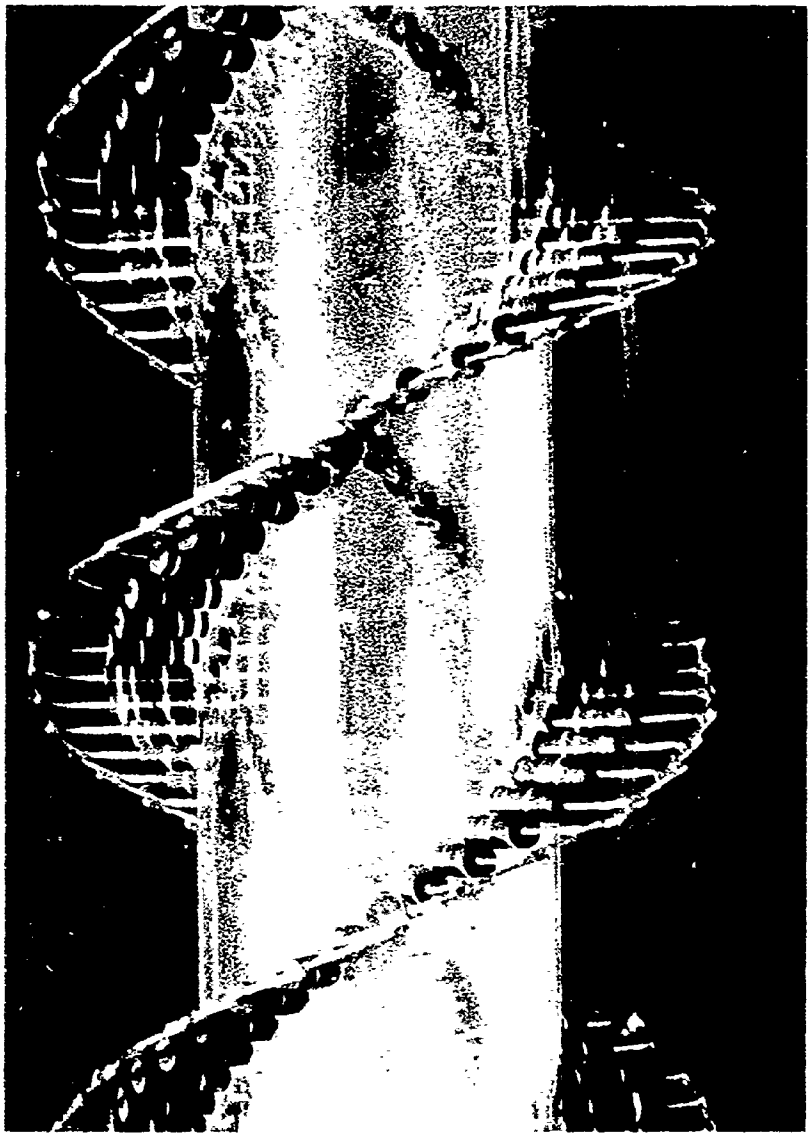

which made the laser cavity stable.

As previously mentioned the laser medium was excited using an electrical discharge transverse to the laser axis. This was accomplished using two helical electrodes in the acrylic laser tube as shown in the photograph of Figure 3-2. Each electrode consisted of a helical distribution of resistors around the tube. Each helix had a pitch of 6 inches and there were 36 resistors every 6 inches as measured along the tube axis. The electrode to which the high voltage was applied consisted of 1000 Ω resistors in parallel and the grounded electrode consisted of 47 Ω resistors. The leads of the resistors were all cut to the same length and were cut at an angle to give a sharp edge. The separation between the ends of opposing resistors in the acrylic tube was 1.25 inches. The resistors were glued into holes drilled into the acrylic tube with a #64 drill, with Emerson epoxy. In order to get a uniform discharge in the laser tube it was found necessary to join each helix with the center conductor of a piece of RG-8U cable after every revolution of that helix about the tube. These pieces of cable can be seen at the bottom of the laser in Figure 3-2.

The laser medium consisted of a mixture of the gases, carbon dioxide, helium and nitrogen. The roles of each of these gases in the carbon dioxide laser can best be understood by referring to Figure 3-3 which shows a few of the lower vibrational levels of the carbon dioxide molecule and the nitrogen molecule. The CO_2 molecule is a linear symmetric molecule which has three fundamental modes of oscillation as shown in Figure 3-4. The laser transition occurs between the first energy level of the assymmetric mode (0,0,1) and the

Figure 3-3: Lower vibrational levels of the carbon dioxide molecule and the nitrogen molecule

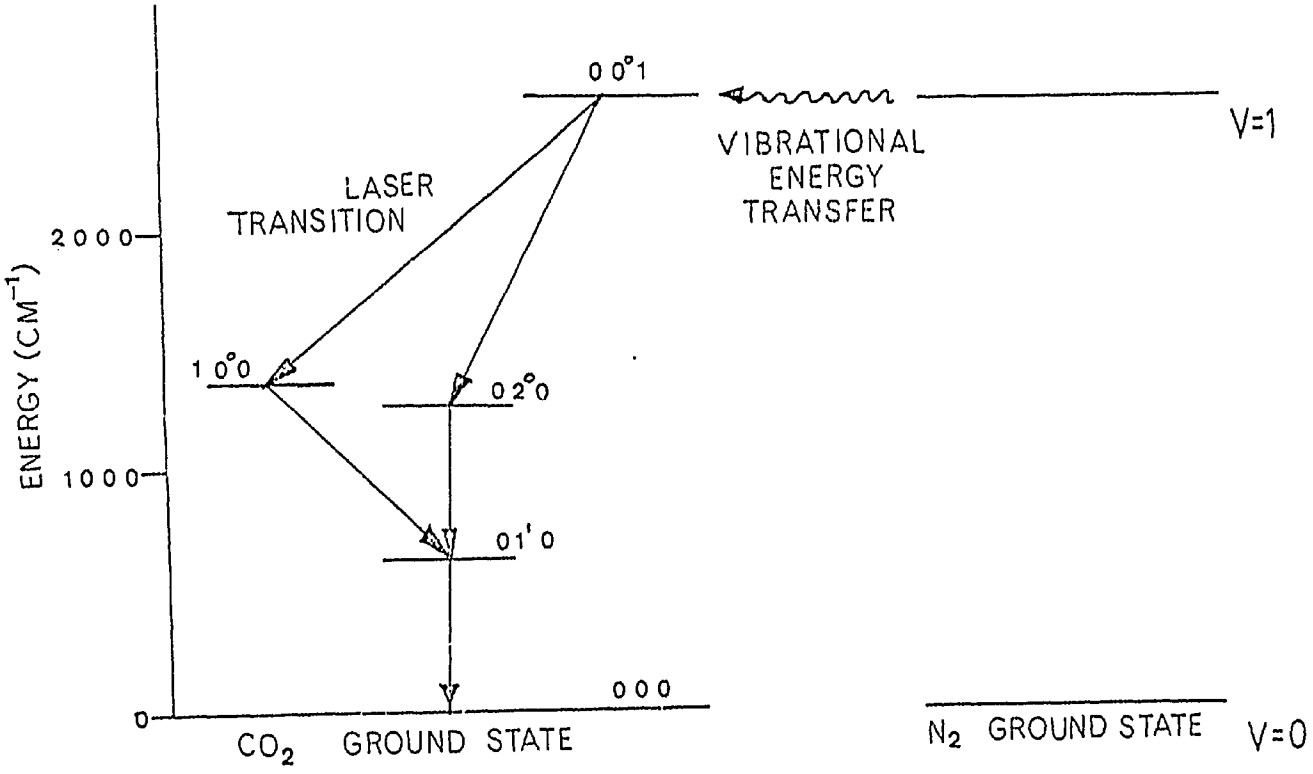
00°1
V=1
VIBRATIONAL
ENERGY
TRANSFER
LASER
TRANSITION
2000
ENERGY (CM⁻¹)
10°0
02°0
1000
01'0
000
0
CO2 GROUND STATE
N2 GROUND STATE
V=0

Figure 3-4: Vibrational modes of the carbon dioxide molecule

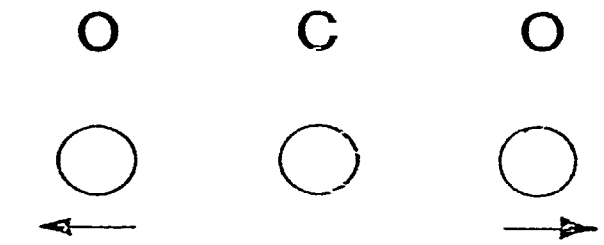

SYMMETRICAL

ν_1 O O

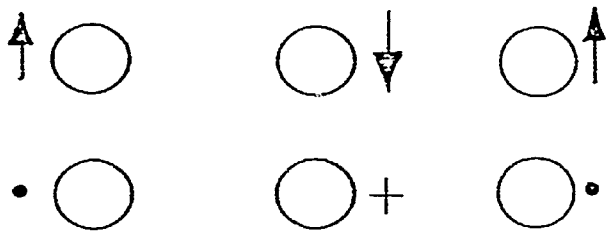

DEFORMATIONAL

O ν_2 O

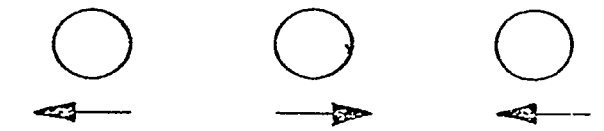

ASYMMETRIC

O O ν_3

Figure 3-5: Laser output power as a function of time

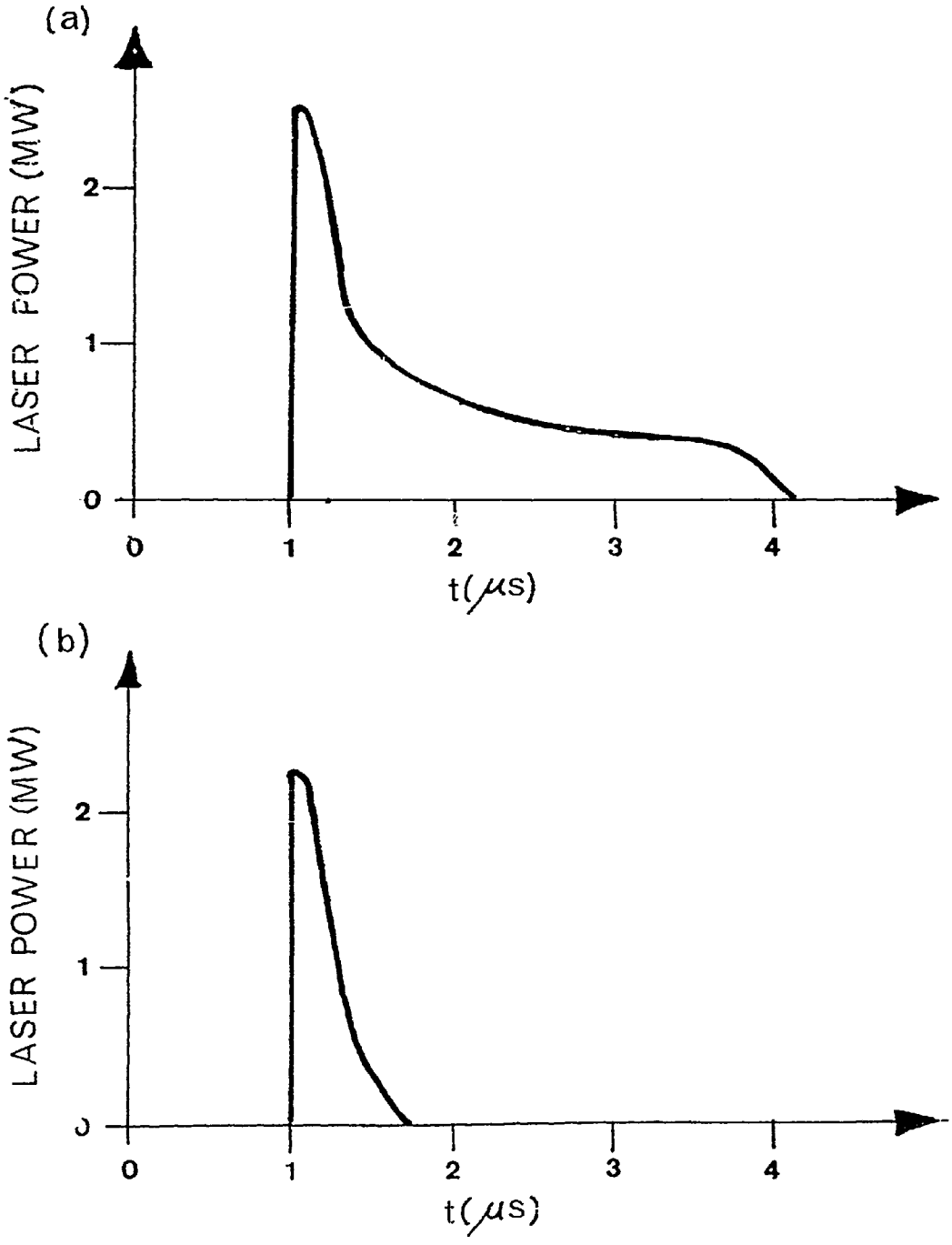
(a)
LASER POWER (MW)
2
1
0
0
1
2
3
4
t(μs)
(b)
LASER POWER (MW)
2
1
0
0
1
2
3
4
t(μs)

Figure 3-6: Schematic diagram of the laser charging and discharging circuit

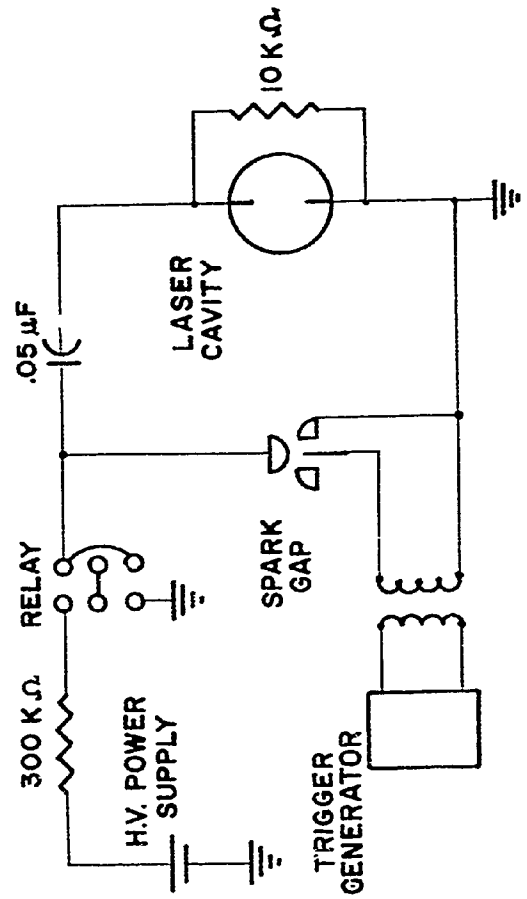
10 KΩ
LASER CAVITY
.05 μF
SPARK GAP
RELAY
300 KΩ
H.V. POWER SUPPLY
TRIGGER GENERATOR

first level of the symmetric mode (1,0,0), as shown in Figure 3-3. Nitrogen is added to the discharge because there is a very efficient energy transfer from the first vebrational level of the nitrogen molecule to the upper laser level. Helium is added because it helps to improve the discharge and it also helps to depopulate the lower CO_2 vibrational levels which can act as a bottleneck for the effective transfusing of molecules down to the ground state.

The relative proportion of the gases in the laser mixture helped determine the output characteristics of the laser pulse. The gas pressure in the laser cavity also affected the laser pulse shape. A gas mixture containing a substantial percentage of N_2 such as 80% helium, 10% CO_2 and 10% N_2 resulted in a pulse like that shown in Figure 3-5(a). It consisted of an initial spike of power ~2 MW and FWHM 180 ns followed by a lower power tail (~.5 MW) lasting for several microseconds. The energy in the initial spike comes mainly from direct electron collisional excitation of the upper laser level whereas the energy in the tail is due to the transfer of energy between the first vibrational level of N_2 and the upper laser level. By omitting the N_2 and having a mixture such as 90% He and 10% CO_2 only the initial spike is obtained as shown in Figure 3-5(b).

The operating pressure in the laser was in the range from 100 Torr to 600 Torr ans was operated as a closed system. The optimum gas pressure for laser power and energy was found to be ~450 Torr.

The charging and discharging circuit for the laser are shown schematically in Figure 3-6. The capacitor was a 0.05 uF capacitor supplied by condensor Products. It was rated at 50 KV and charged to 40 KV. Charging was by a 70 kV 5.5 mA constant current power supply

Figure 3-7: Circuit diagram for the trigger generator

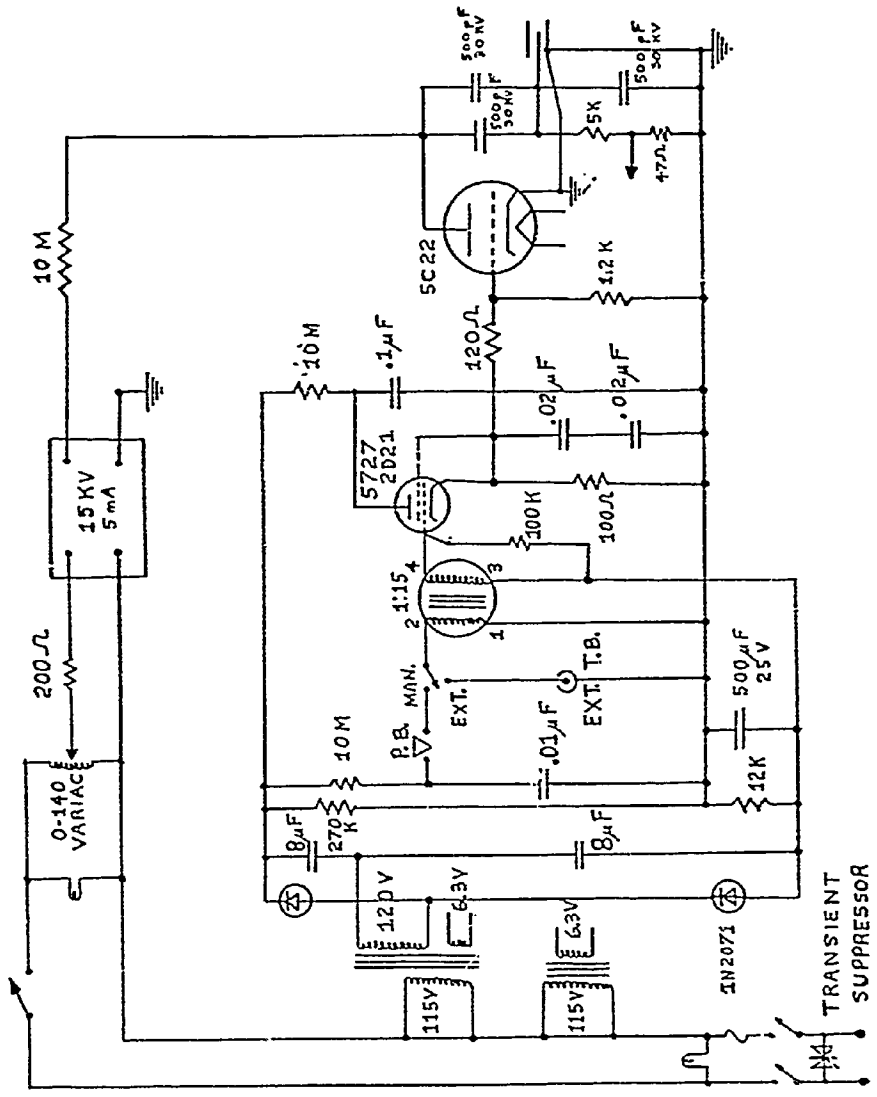
10 M
15 KV
5 mA
200Ω
0-140
VARIAC
10 M
.1μF
120Ω
5C22
1.2 K
5K
47Ω
500pF
30 KV
.02μF
.02μF
5727
2D21
100K
100Ω
1:15
P.B.
MAN.
EXT.
.01μF
EXT.
T.B.
500μF
25V
12K
10 M
270 K
8μF
8μF
12 V
6.3V
6.3V
115V
115V
1N2071
TRANSIENT
SUPPRESSOR

Figure 3-8: The discharge current through the laser and the output power of the laser as a function of time

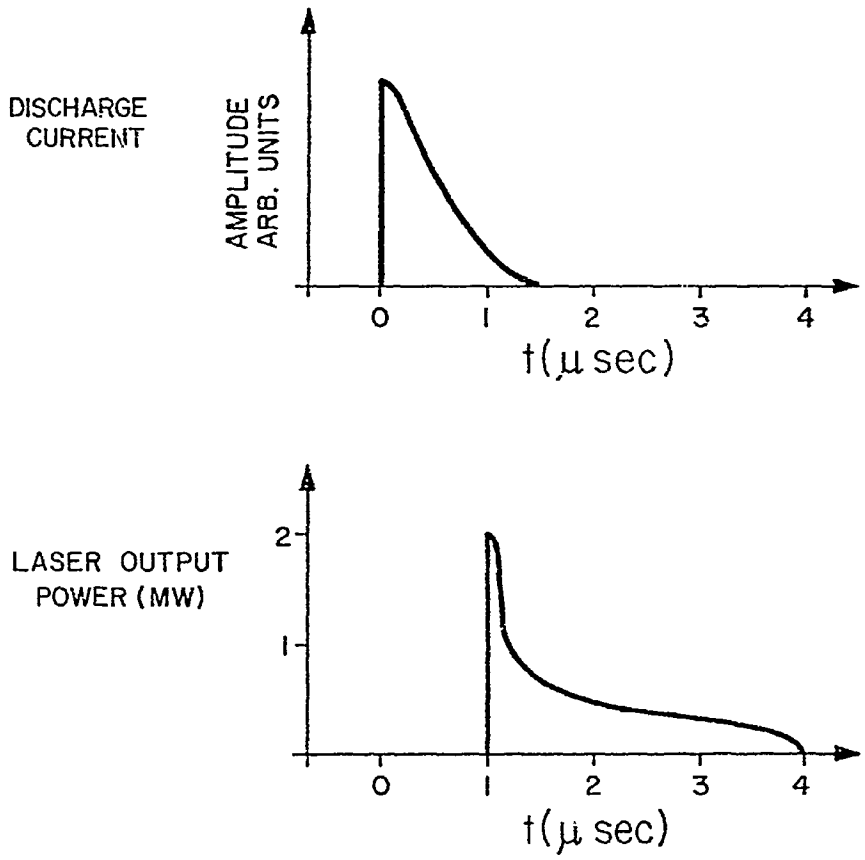
DISCHARGE CURRENT
AMPLITUDE ARB. UNITS
0
1
2
3
4
t(μ sec)
LASER OUTPUT POWER (MW)
2
1
0
1
2
3
4
t(μ sec)

Figure 3-9: Schematic diagram for the shock tube charging and discharging circuit

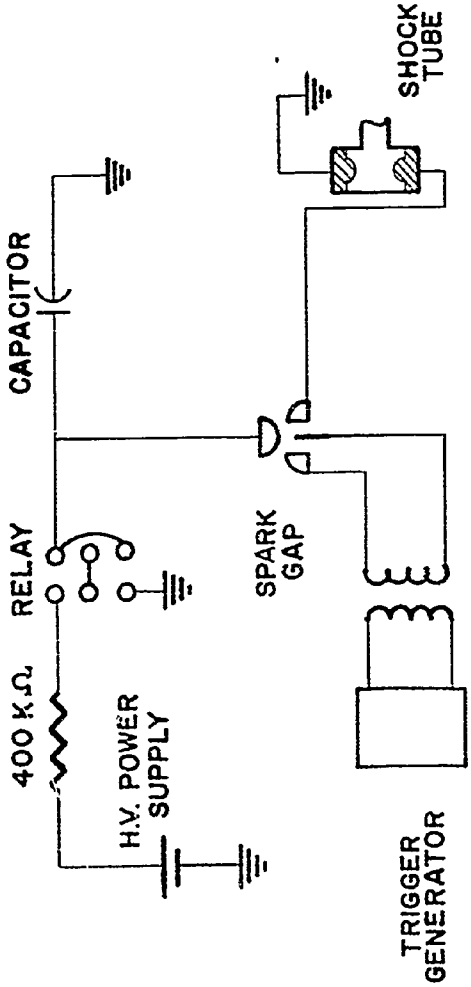
SHOCK TUBE
CAPACITOR
RELAY
SPARK GAP
400 K.Ω.
H.V. POWER SUPPLY
TRIGGER GENERATOR

made by Universal Voltronics. The capacitor discharge was triggered by a spark gap switch using a pulse from a 15 kV trigger generator through an isolation transformer. A circuit diagram of the trigger generator is shown in Figure 3-7. The isolation transformer was a six turn coil of RG/8U coaxial cable with each turn having a diameter of approximately 15 cm. The inner conductor of the cable was used as the primary coil and the outer one as the secondary coil. The operating efficiency of the laser was about 4%. The discharge current through the laser was critically damped and had a duration of ~1 μs. In Figure 3-8 is shown the discharge current through the laser and the output power of the laser as a function of time.

3.2 The Electromagnetic Shock Tube

The plasma studied in this experiment was produced in an electromagnetic shock tube of the type first developed by Fowler et al [24,25] and also studied later by Kolb [26] and McLean et al [27,28].

A schematic diagram of the shock tube set up is shown in Figure 3-9. The plasma was formed in the shock tube by discharging the capacitor through the tube. The capacitor was a 8 μF, 5 nH Tobe capacitor rated at 25 KV. It was charged by a 32 KV, 10 mA constant current Universal Voltronics power supply. The capacitor was discharged using a trigger generator and a spark gap in the same way as already described for the carbon dioxide laser. In the heating experiment the plasma was formed by a 10 kV discharge between the electrodes in the shock tube. The discharge causes rapid heating and a subsequent expansion of the gas in the shock tube resulting in the formation of a shock wave which propagates down the tube. The $\bar{J}x\bar{B}$ force of the circuit current interacting with the plasma further enchances the shock speed. Shown in

Figure 3-10: Schematic diagram of the shock tube and the interaction chamber

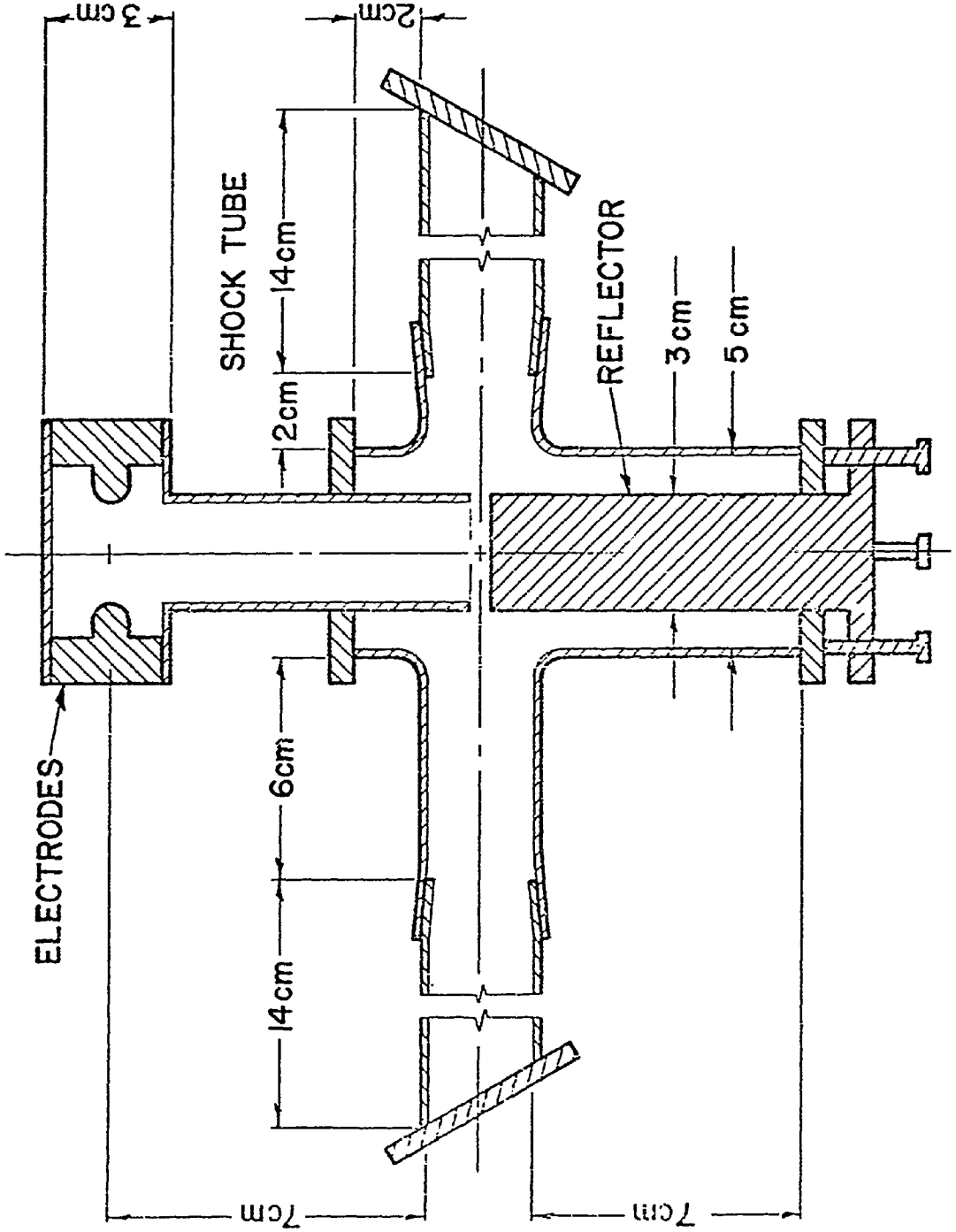
3 cm
2cm
SHOCK TUBE
14cm
2cm
REFLECTOR
3cm
5 cm
ELECTRODES
6cm
14cm
7cm
7cm

Figure 3-10 is a schematic diagram of the shock tube and the laser plasma interaction chamber. Both the shock tube and the interaction chamber were made of pyrex. The electrode and the reflector were made of nickel. The brewster angle entrance and exit windows were sodium chloride flats.

The plasma was formed from helium at a filling pressure in the range 1 to 5 torr. The plasma moving down the shock tube is a mixture of plasma from the discharge region of the shock tube and plasma created by the shock wave. The shock velocity, v, decreases as it propagates down the tube, decreasing rapidly over the first several centimeters and for larger distances, d, $v \alpha d^{-\frac{1}{2}}$. The shock velocity could be increased by increasing the discharge voltage V, and by decreasing the filling pressure p. For a given value of V, $v \alpha p^{-\frac{1}{2}}$.

Shock velocities of ~3 cm/μs were easily obtained in the T-tube, however it should be mentioned that the Rankine-Hugoniot relations [27] could not be used to predict the electron temperature or density behind the shock front. McLean et al [27] compared the temperature and density behind the shock obtained from spectroscopic measurements with the values calculated using the Rankine-Hugoniot equations. They found that the shock relations gave a temperature too low by a factor of two and a density too high by a factor of 3. One reason for the discrepancy is that the plasma is partly composed of plasma from the discharge region, which was not created by the shock wave.

On reaching the end of the T-tube, the incident shock was reflected back into the plasma already produced by the incident shock. The plasma behind the reflected shock had both a higher temperature and a higher density than the plasma behind the incident shock.

Figure 3-11: Paths of plasma particles before and after the incident and reflected shock according to simple shock theory

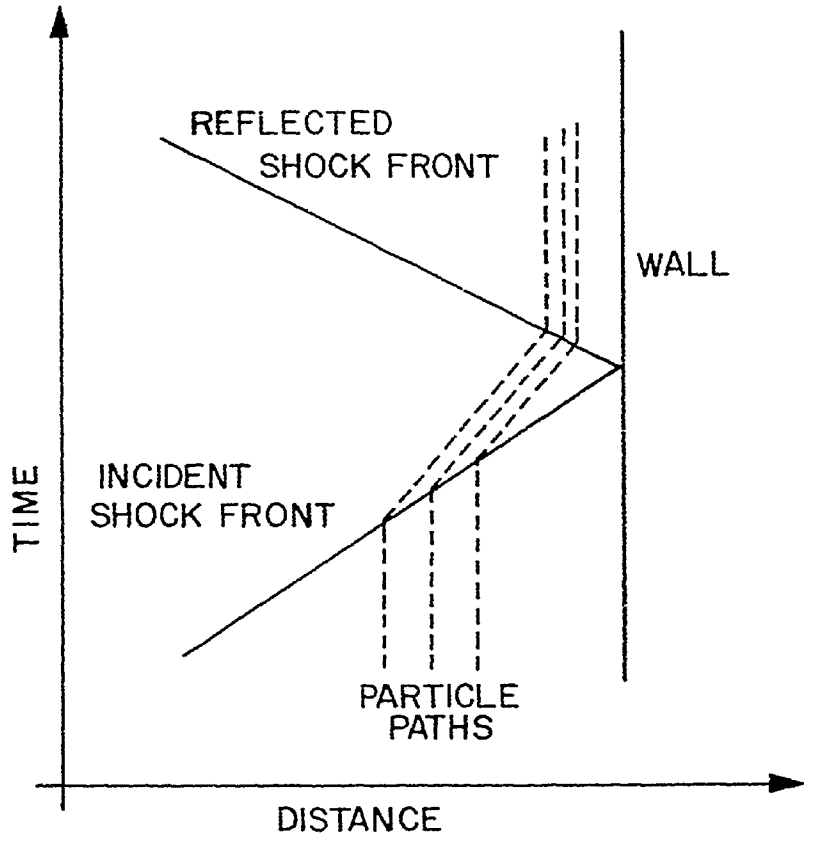
REFLECTED
SHOCK FRONT
WALL
INCIDENT
SHOCK FRONT
TIME
PARTICLE
PATHS
DISTANCE

Figure 3-12: Photographs of the plasma at various times during its developement

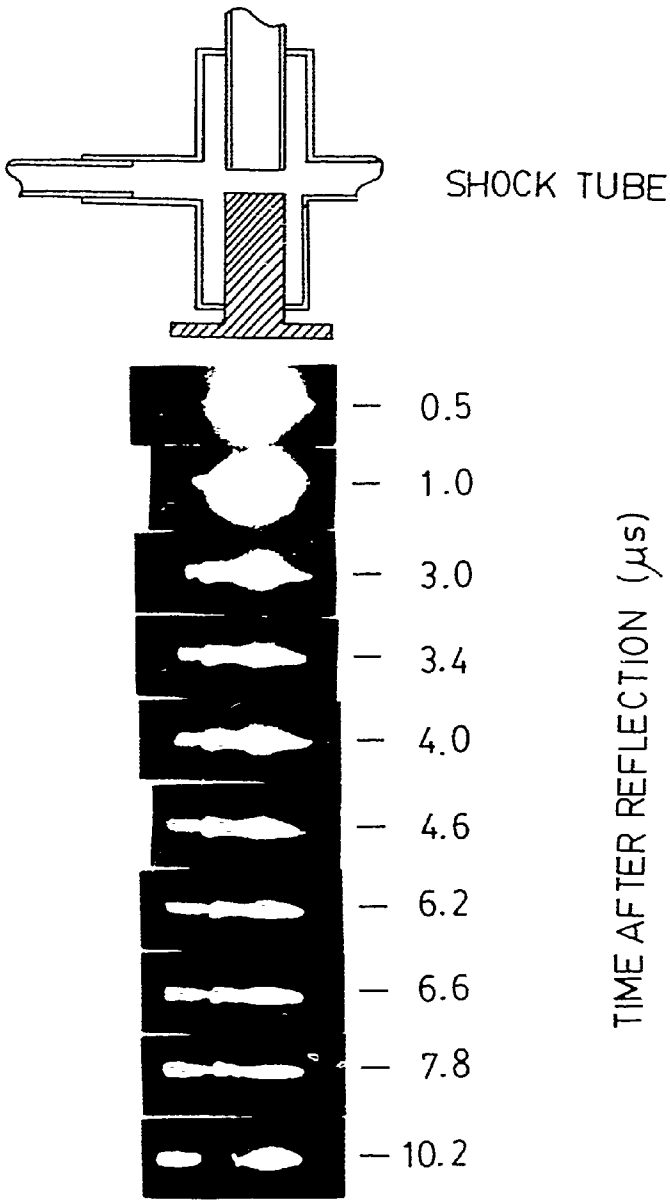
SHOCK TUBE
0.5
1.0
3.0
3.4
4.0
4.6
6.2
6.6
7.8
10.2
TIME AFTER REFLECTION (μs)

According to elementary shock wave theory [29] the plasma behind the incident shock follows the shock front at a velocity somewhat less than the shock velocity but after reflection at a plane boundary the plasma behind the reflected shock is at rest, as shown in Figure 3-11. The temperature and density behind the reflected shock were also more uniform in the radial direction, than was the incident shock [30].

Since there is a gap between the open end of the shock tube and the reflector, the plasma rapidly expanded into the interaction chamber and also down the sidearms of the interaction chamber. From measurements of the velocity of the luminous front in the sidearm it was established that the plasma was moving faster than a sound wave in helium, so the plasma in the sidearms was also a shock plasma.

Shown in Figure 3-12 are photographs of the plasma at various times during the plasma evolution.

The temperature and density of the plasma as a function of time as well as the methods by which these values were obtained will be discussed in detail later. It was found that the plasma formed by the incident shock wave had a maximum electron density of $\sim 3 \times 10^{17} cm^{-3}$ and a maximum electron temperature of ~3.5eV. The plasma behind the reflected shock had a maximum electron density of $\sim 10^{18} cm^{-3}$ and a maximum temperature of ~4.0eV.

3.3 The Detection System

3.3.1 Plasma Light Detection

A. High Speed Photography

An image converter camera was used to photograph the plasma in visible light at various times during its development. The camera used

Figure 3-13: Circuit diagram for the voltage divider base for the photomultiplier

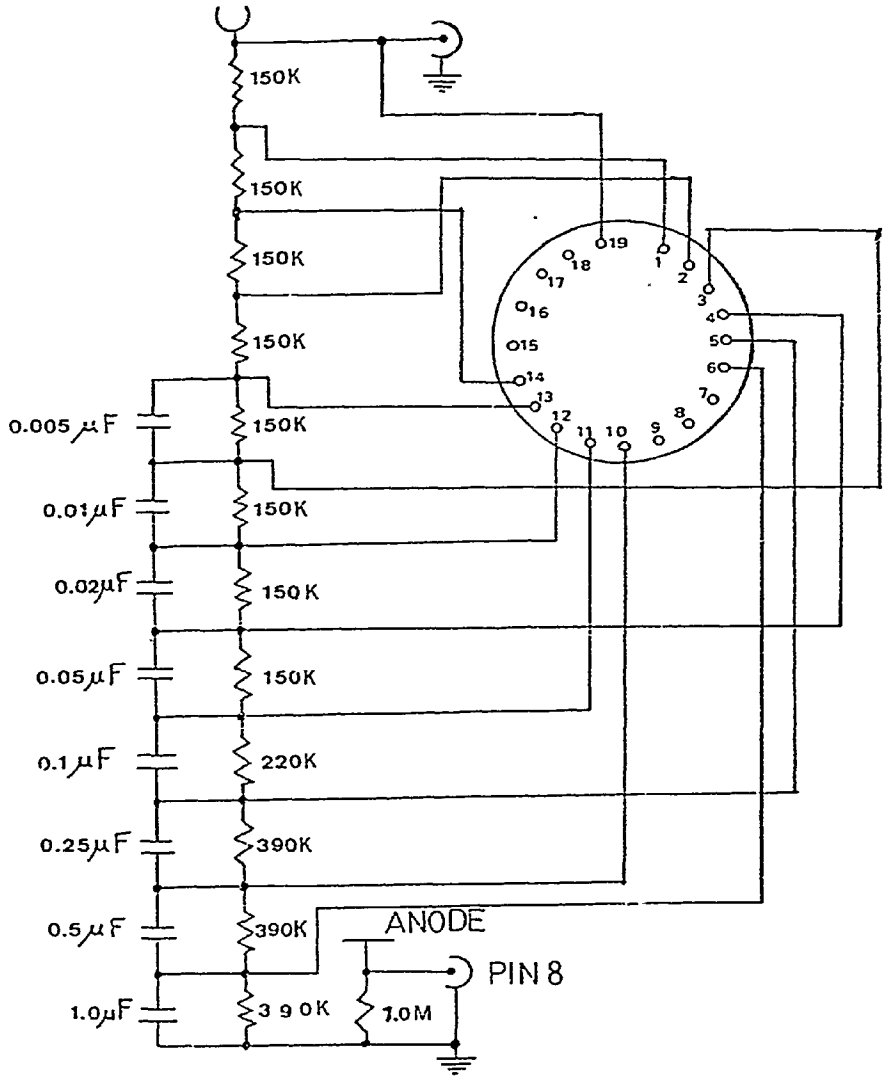
150K
150K
150K
150K
150K
150K
150K
150K
220K
390K
390K
390K
1.0M
0.005μF
0.01μF
0.02μF
0.05μF
0.1μF
0.25μF
0.5μF
1.0μF
ANODE
PIN 8
19
1
2
3
4
5
6
7
8
9
10
11
12
13
14
15
16
17
18

was an Abtronics Model 2 electronic camera supplied by Abtronics Inc. of Livermore California. It was a single frame camera with exposure times of 0.01, 0.1 and 1.0 μs. The camera was equipped with a delayed triggering system which allowed synchronization of the camera with other systems. The time delay between trigger input and camera activation could be continuously varied in the range 0.2 μs to 100 μs. The built in optical system of the camera permitted focussing from approximately 20 cm to infinity.

B. The Monochromator and Photomultiplier

Spectroscopic observations of the plasma were made using a monochromator in conjunction with a photomultiplier. The monochromator used was a Heath Model EV700-70 with a f/6.8 aperture. Resolving power of better than 1 Å could be obtained using suitable choices for slit height and width. The slit width could be varied continuously from 5 micrometers to 2 mm. The monochromator was equipped with a grating having 1180 lines/mm and a blaze wavelength of 2500 Å. The wavelength range of the monochromator was from 1900 Å to 10000 Å with a wavelength accuracy of ± 1 Å.

The photomultiplier used in conjunction with the monochromator was an EMI model 9558B. The cathode had an S-20 response which gave a quantum efficiency of ~20% near 4000 Å, decreasing to ~10% at 6000 Å. The photomultiplier was operated at a voltage of about 1000 V, supplied by a Fluke type 415B regulated power supply. Shown in Figure 3-13 is a circuit diagram of the voltage divider base for the photomultiplier. At the operating voltage of 1000 volts the dark current was less than 10 nA. The photomultiplier response was found to be

linear for up to 2 mA output and all measurements were made in the linear region. The photomultiplier was also enclosed in an antimagnetic shield to cut down on noise.

3.3.2 Laser Beam Detection

A. Energy Detection

The energy of the laser pulse was measured with a pyroelectric detector supplied by Gen-Tec Inc. of Dalton Quebec. The detector was a Model Ed-200 fast response joulemeter which had a sensitivity of 11 volts/joule for the load impedance of 10^6 ohms of the Tektronix oscilloscope on which its signal was displayed. It was impedance matched to a 50 ohm coaxial cable so it could be directly connected to the oscilloscope using RG58-U cable. The response time of the detector was 5 ms and the recovery time was 300 ms. Laser energies from 2 J to 1.0 mJ could be measured.

B. Power Detection

The power output of the laser as a function of time (ie. its pulse shape) was monitored using a photon drag detector [31].

The photon drag detector operation is based on the transfer of photon momentum to electrons or holes. When CO_2 laser radiation is incident on germanium some of the radiation is reflected but most enters the germanium crystal. Some of the photons in the laser beam are absorbed by the free carriers (electrons or holes) and they acquire momentum from the photons and are driven through the crystal in the direction of the laser beam. A voltage, therefore appears in the crystal in the direction of the laser beam. This voltage can be

Figure 3-14: Schematic diagram and photograph of the photon drag detector

(a)

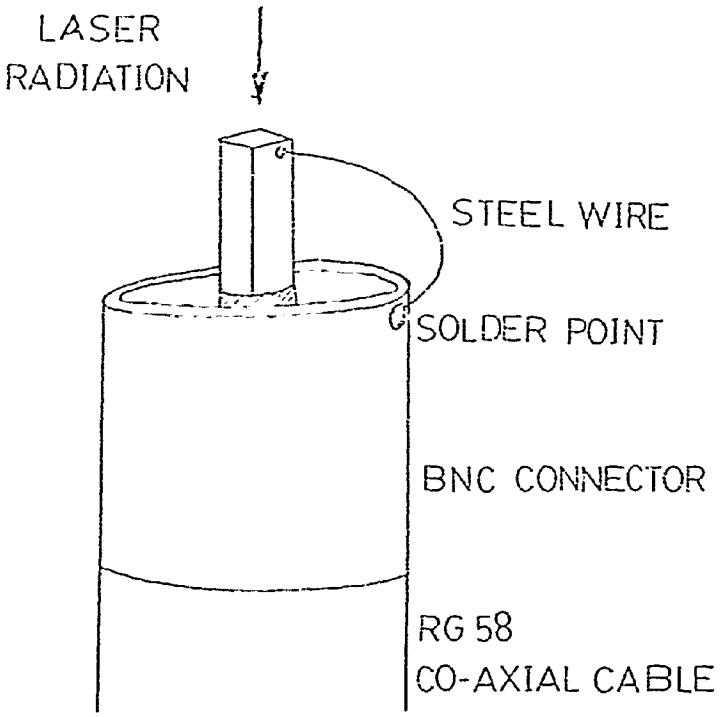
LASER
RADIATION
STEEL WIRE
SOLDER POINT
BNC CONNECTOR
RG 58
CO-AXIAL CABLE

(b)

monitored on an oscilloscope thus giving a signal corresponding to the laser power.

The detector was constructed from rectangular prisms of p-type germanium 0.1 cm x 0.1 cm x 1.0 cm. supplied by Semi Metals of Westbury, New York. The germanium prism was attached to the center conductor of a BNC connector as shown in Figure 3-13. A thin steel wire was soldered to a point on the side of the prism just below the square end face furthest from the BNC connector. The other end of the steel wire was soldered to the outer conductor of the BNC connector. The area of the space between the steel wire and the germanium prism had to be kept as small as possible in order to reduce noise. The CO_2 laser beam was focussed onto the end of the germanium prism (Figure 3-14). The BNC connector was connected to the oscilloscope using a short (<50 cm) RG62-U coaxial cable.

For p-type germanium the sensitivity of the detector for 10.6 μ radiation is given by [32]

$$S = \frac{0.6 \times 10^{-7}\rho}{A}\left[1-e^{-2L/\rho}\right] \quad \text{volts/watt}$$

where ρ is the resistivity of the germanium in ohms/cm

L is the length of the germanium in cm

A is the area of the crystal's face in cm^2

The values of these quantities for our detector were L = 1 cm $\rho = 100\Omega/cm$ $A = .01cm^2$.

Therefore

$S = 1.2 \times 10^{-5}$ volts/watt

= 12 mV/kW

However some of the laser beam is reflected at the front surface of the detector so the response is somewhat less than this. Nevertheless for CO_2 lasers of powers ~1000 KW a very respectable signal is obtained, in our case ~2 volts.

The response time of the detector is theoretically the momentum relaxation time of the charge carriers which is about 3×10^{-13}s, however this is limited by the resistance of the detector and the input capacitance of the scope. In our case the capacitance C was 20 pF so $RC \approx 2$ ns which is still extremely good for our purposes.

Photon drag detectors are very convenient for use with high power CO_2 lasers since they can operate at room temperature and in addition since they don't require a power source noise problems are greatly reduced.

CHAPTER 4: PLASMA HEATING BY THE LASER

4.1 The Experimental Set-Up

The experimental set-up is shown in Figure 4-1. M_1 and M_2 are the laser mirrors. M_3 is a first surface aluminum mirror. After reflecting from M_3 the laser beam passed through a sodium chloride flat which reflected about 10% of the laser beam onto a germanium photon drag detector which monitored the output of the laser. The main laser beam was finally focussed by a mirror, M_4, of focal length 80 cm into the interaction chamber. The beam focus was mid-way between the end of the shock tube and the shock tube reflector. The diameter of the focussed beam was ~3 mm and since M_4 had a long focal length the beam diameter did not change appreciably over the interaction region. The distance between the end of the shock tube and the reflector was set at 4 mm. Laser radiation emerging from the interaction chamber was transmitted through the germanium flat onto the pyroelectric energy detector. Any laser light reflected from the germanium was absorbed by the neutral density filters shown in the diagram.

The plasma was observed along the same axis as that of the laser beam. The germanium flat reflected most of the visible light from the plasma; the light then passed through neutral density filters

Figure 4-1: Schematic diagram of the experimental set up for the heating experiment

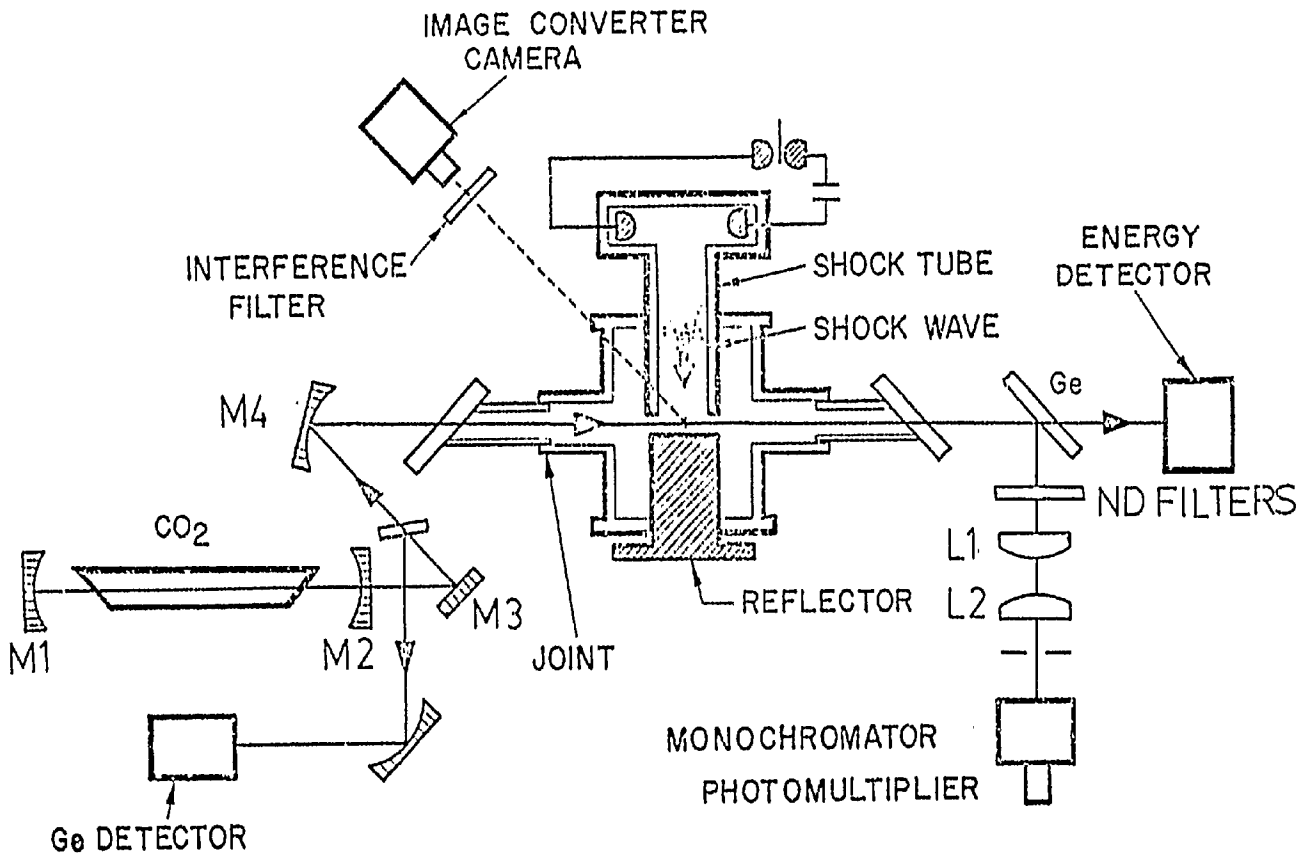
IMAGE CONVERTER
CAMERA
INTERFERENCE
FILTER
SHOCK TUBE
SHOCK WAVE
ENERGY
DETECTOR
M4
Ge
ND FILTERS
L1
L2
CO_2
M1
M2
M3
JOINT
REFLECTOR
MONOCHROMATOR
PHOTOMULTIPLIER
Ge DETECTOR

and two lenses L_1 and L_2 onto the monochromator. Neutral density filters were used to keep the light intensity low enough so that the photomultiplier operated in its linear region.

The image converter camera was used in conjunction with an interference filter to photograph the plasma.

4.2 Alignment of the Detection Optics

The lenses L_1 and L_2 had to be aligned so as to image the laser-plasma interaction region onto the slit of the monochromator. A strong white light source was used to illuminate the end of the shock tube and the nickel reflector. Lens L_1 was placed a distance (measured along the axis of the system), equal to its focal length from the centre of the interaction region. L_2 was then adjusted until a sharp image of the shock tube and the reflector was seen on the entrance to the monochromator. By adjusting L_1 and L_2 any region between the shock tube and the reflector could be imaged on the entrance slit of the monochromator. Usually the point midway between the shock tube and the reflector was observed. A He-Ne laser was then aligned along the path of the CO_2 laser beam with mirror M_2 removed. This visible laser beam was used to simulate the invisible CO_2 laser beam. It was found that the path of the He-Ne laser was an excellent approximation to the path of the CO_2 laser beam. Mirrors M_3 and M_4 were adjusted so that the He-Ne beam passed through the proper region between the shock tube and the reflector. A small piece of ground glass was placed in the laser beam between the reflector and the shock tube. The image of this brilliantly illuminated ground glass was observed to ensure that it was falling on the entrance slit of the monochromator. The ground glass was then removed and mirror M_2 was

Figure 4-2: Block diagram showing the method of snychronizing the laser and the plasma

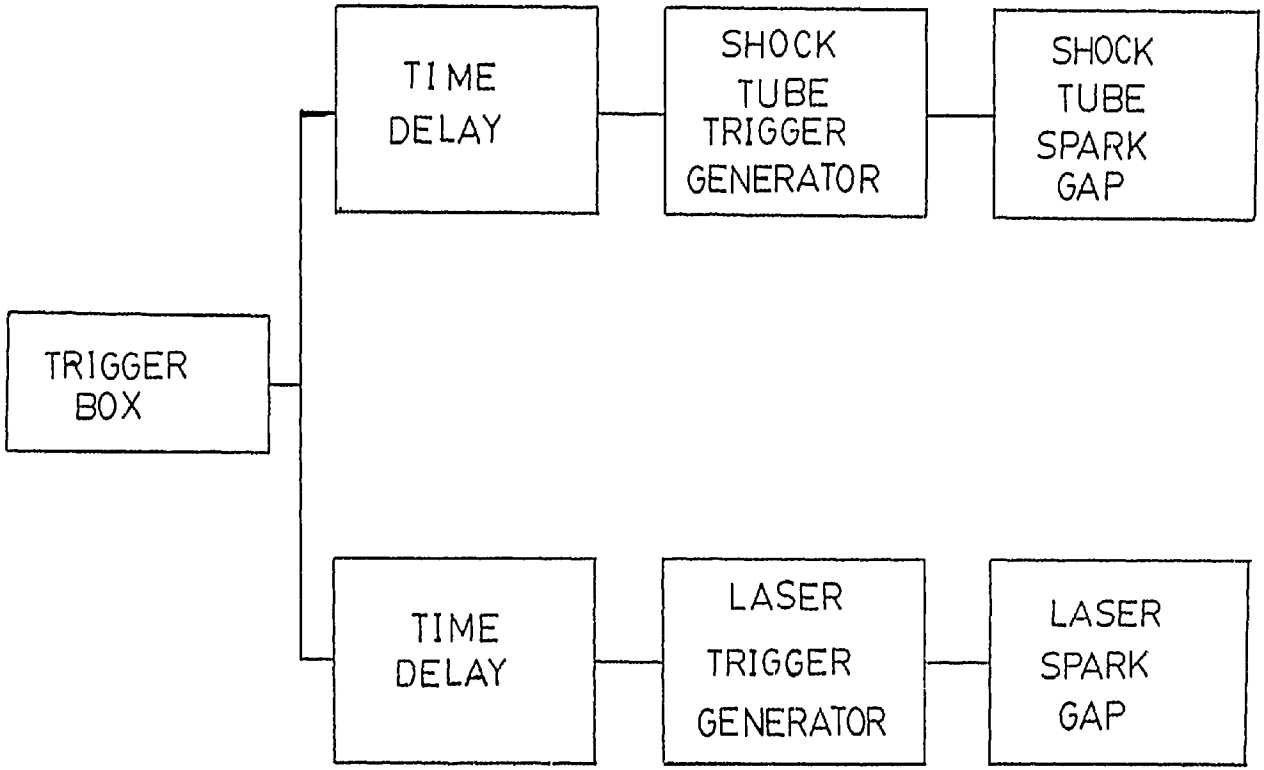
TRIGGER BOX
TIME DELAY
SHOCK TUBE TRIGGER GENERATOR
SHOCK TUBE SPARK GAP
TIME DELAY
LASER TRIGGER GENERATOR
LASER SPARK GAP

Figure 4-3: Circuit diagram for the time delay unit used in synchronizing the laser and the plasma

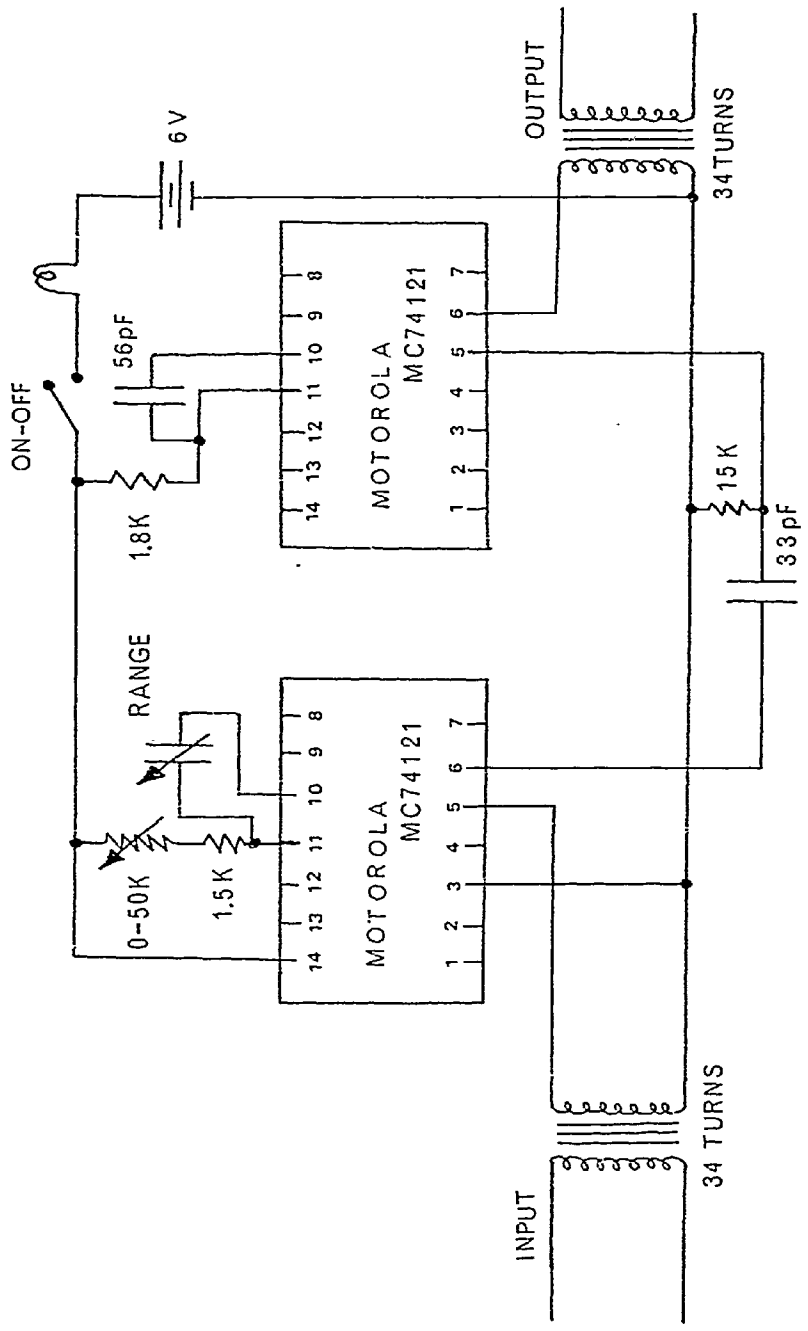
6 V
ON-OFF
56pF
1.8K
RANGE
0-50K
1.5K
MOTOROLA
MC74121
MOTOROLA
MC74121
OUTPUT
34TURNS
15 K
33pF
INPUT
34 TURNS

returned. The CO_2 laser was then aligned using the He-Ne beam. In this way we were sure that we were imaging the plasma, through which the laser beam had passed, onto the slit of the monochromator.

4.3 Synchronization of the Plasma and the Laser

Synchronization of the plasma and the laser was accomplished using two time delay units as shown schematically in Figure 4-2. A signal from a hand operated trigger box was fed into both time delay units. Each time delay could be varied from .5 μs to 500 μs. The output signal from each time delay then triggered their respective trigger generators. With this simple set up it was possible to adjust the time, in the evolution of the plasma, at which the laser beam would arrive.

A circuit diagram of the time delay is shown in Figure 4-3.

4.4 Plasma Diagnostics

Spectroscopic measurements were used to determine the basic plasma parameters. Spectrally resolved measurements of a stark broadened HeI line at 5876 Å were used to determine the electron density. The electron temperature was measured using the ratio of the intensities of two spectral lines.

For about the first three microseconds after formation of the reflected shock, the temperature of the plasma was measured using the ratio of the intensities of the HeII line at 4686 Å to the HeI line at 5876 Å [33]. The ratio of the intensities was found using two methods, both of which gave the same temperature. One method consisted of measuring the profile of each line separately. The

Figure 4-4: Intensities of the HeI line at 5876 Å and the HeII line at 4686 Å as a function of time

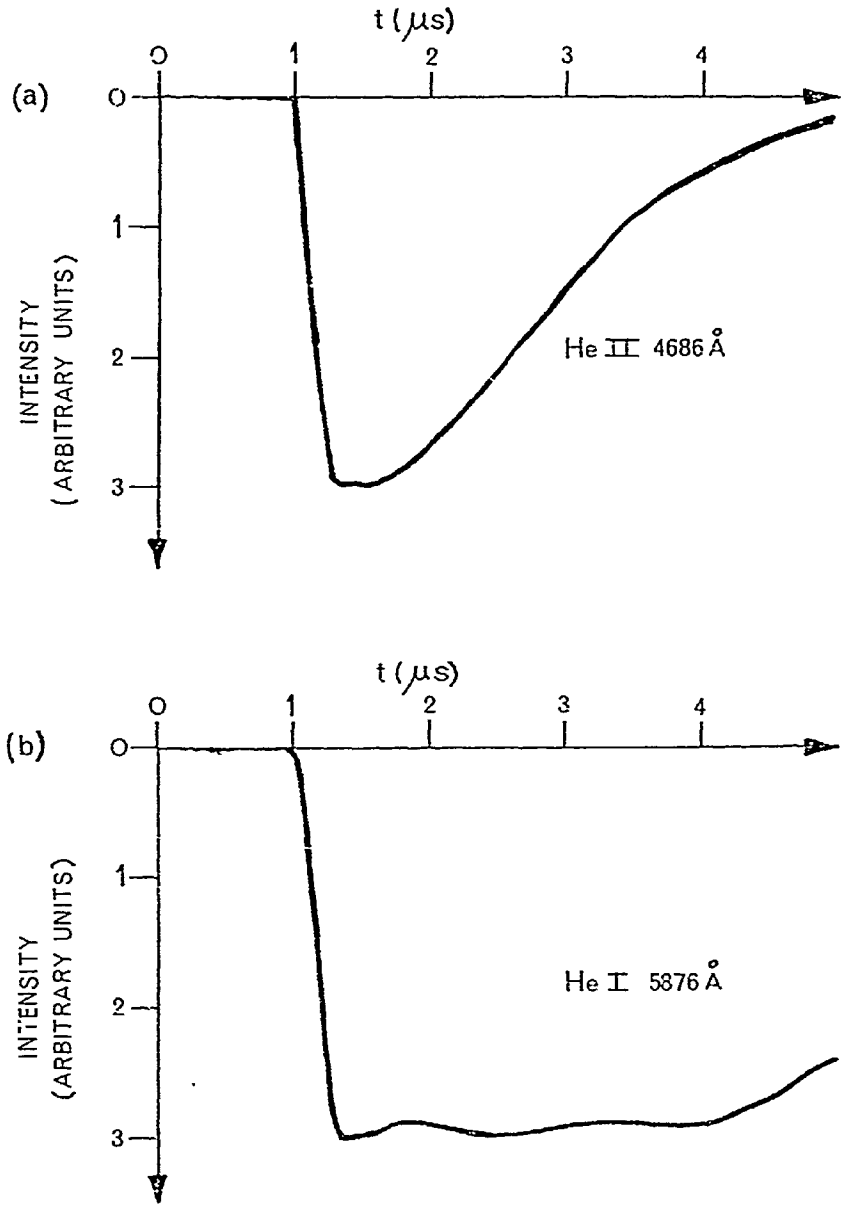
t (μs)
0
1
2
3
4
(a)
0
1
2
3
INTENSITY
(ARBITRARY UNITS)
He II 4686 Å
t (μs)
0
1
2
3
4
(b)
0
1
2
3
INTENSITY
(ARBITRARY UNITS)
He I 5876 Å

Figure 4-5: Stark broadened line profiles of the HeI line at 5876 Å and the HeII line at 4686 Å

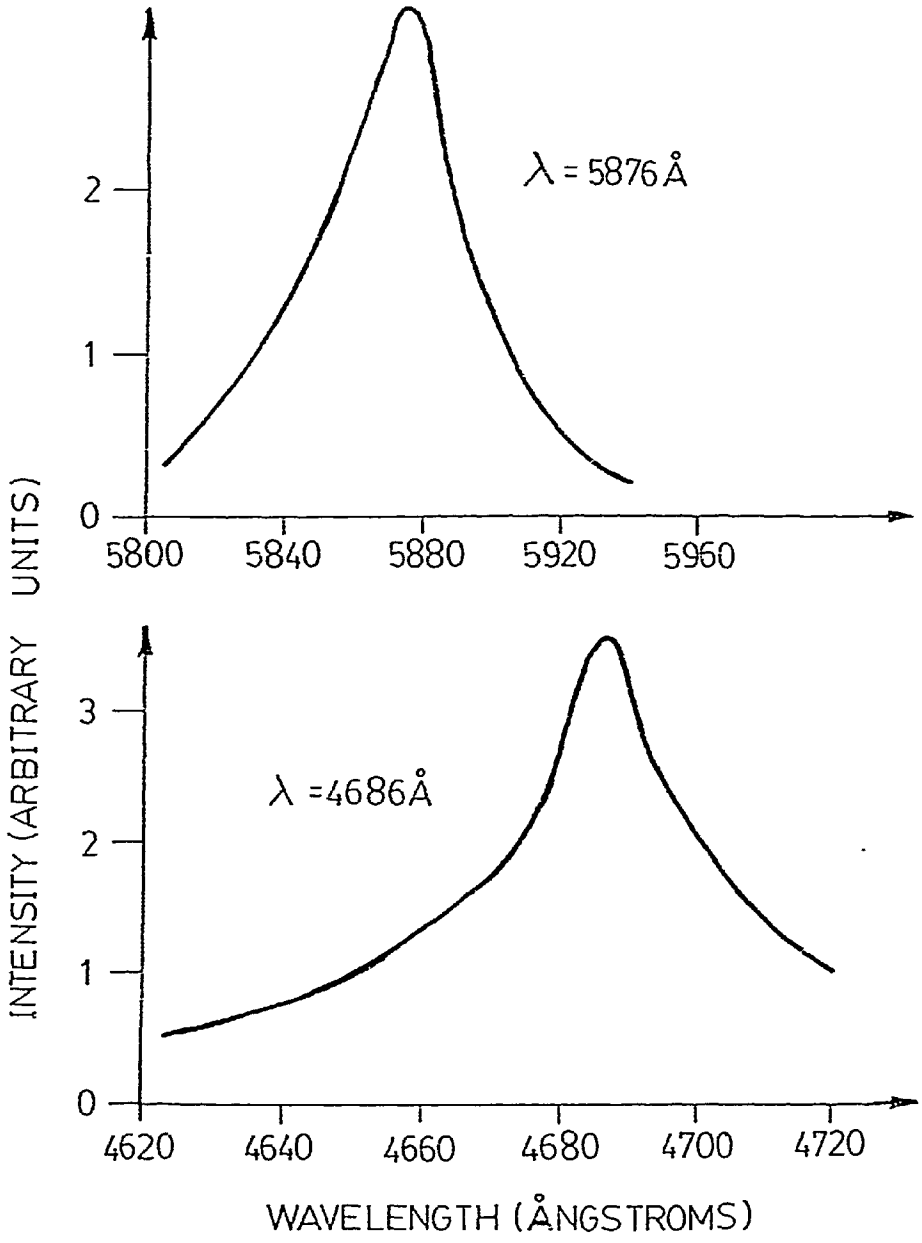
λ = 5876 Å
λ =4686Å
INTENSITY (ARBITRARY UNITS)
0
1
2
3
5800
5840
5880
5920
5960
4620
4640
4660
4680
4700
4720
WAVELENGTH (ÅNGSTROMS)

Figure 4-6: Graph of the intensity ratio of the HeII (4686 Å) line to the HeI (5876 Å) as a function of temperature

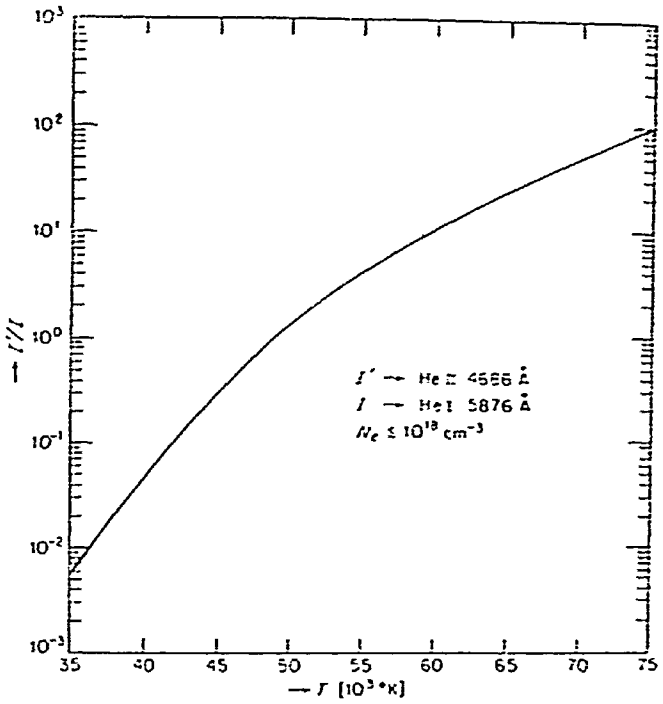
10^3
10^2
10^1
10^0
10^{-1}
10^{-2}
10^{-3}
I'/I
35
40
45
50
55
60
65
70
75
T [10^3 °K]
I' → He II 4686 Å
I → He I 5876 Å
$N_e \leq 10^{13}$ cm^{-3}

profile was obtained 'shot by shot' and the area under each curve was measured to obtain the intensity ratio. The monochromator bandwidth was set to be ≤ 1 Å so the slit width on the monochromator had to be set at 50 microns. Lens L_1 had a focal length of 40 cm and lens L_2 had a focal length of 4 cm. Therefore the area of the plasma being observed was a rectangle ~5 mm x .5 mm. The slit height was always .5 mm.

Figure 4-4 shows typical photomultiplier traces of the intensity of the two helium lines as a function of time.

Shown in Figure 4-5 are the line profiles of the two lines at 0.5 μs after passage of the reflected shock. Before the ratio was calculated the continuum intensity had to be subtracted from each profile and a correction also had to be made for the different sensitivity of the photomultiplier at the two wavelengths.

The electron temperature was then found from the graph of the ratio of the intensities of HeII (4686 Å) to HeI (5876 Å) versus temperature shown in Figure 4-6 [33].

The preceding method of measuring temperature was very time consuming and a simpler method of obtaining the intensity ratios of the lines was used more often. This second method required a knowledge of the width of the spectral lines before it could be applied. The slit width of the monochromator was set large enough so that the bandwidth was sufficiently large so that the entire stark broadened line could be seen in one shot of the plasma. This required a slit width of 0.5 mm and the slit height was again 0.5 mm. Lenses of focal length 50 cm were used for both L_1 and L_2. This resulted in an area .5mm x .5mm of the plasma being observed.

Figure 4-7: The electron temperature and electron density in the reflected shock as a function of time after passage of the reflected shock.

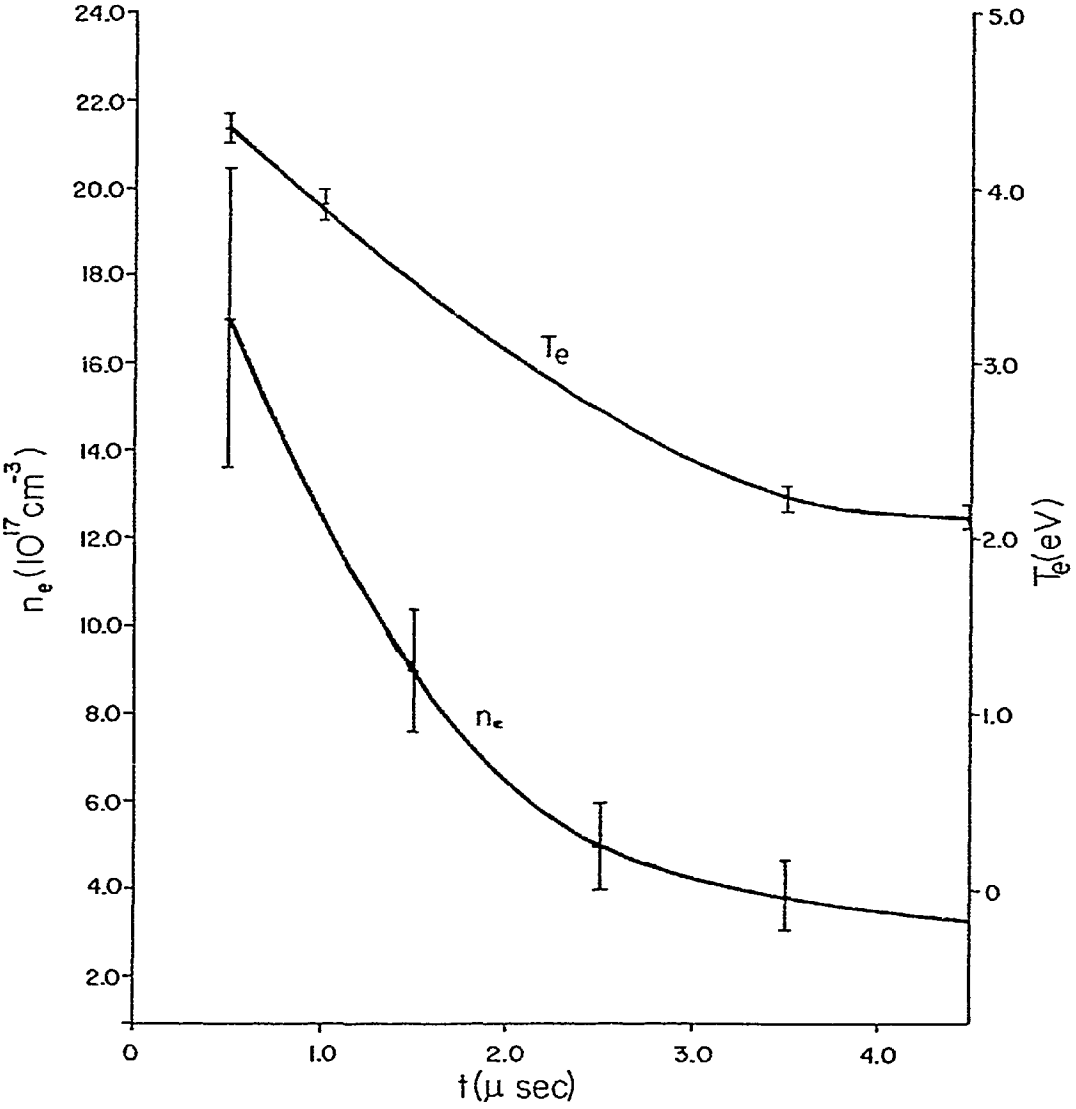
24.0
22.0
20.0
18.0
16.0
14.0
12.0
10.0
8.0
6.0
4.0
2.0
$n_e(10^{17}cm^{-3})$
5.0
4.0
3.0
2.0
1.0
0
$T_e(eV)$
T_e
n_e
0
1.0
2.0
3.0
4.0
t(μ sec)

The electron density was determined by measuring the stark broadened half width of the helium lines, as discussed in Chapter 2. Since the HeI line at 5876 Å was easily measurable for the entire life of the plasma, it was used most often to calculate the density. However when the HeII line at 4686 Å was also observable, it too was used to measure the density. The densities obtained from each line profile always agreed with each other. Figure 4-7 shows the electron temperature and density in the plasma for the first 4 μs after passage of the reflected shock.

During the first few microseconds after reflection from the reflector, the plasma had not yet expanded appreciably into the sidearms so no information is given here on the conditions in the sidearms for times less than 4 μs.

For times greater than ~3 μs after passage of the reflected shock, the temperature of the plasma had dropped to the point where the intensity of the HeII line at 4686 Å was too weak to be measured accurately so Figure 4-6 was no longer useful in calculating the temperature.

In order to discover a suitable method of measuring the electron temperature, the spectrum of the plasma was scanned using the monochromator. It was discovered that one of the impurities in the plasma was silicon possibly due to plasma interaction with the shock tube walls. The large number of silicon lines present offered the possibility that the ratio of the intensities of two silicon lines could be used to determine the electron temperature. In order to use two silicon lines to measure the temperature a number of conditions had to be met. The lines had to be of a sufficient intensity to be easily measured. The

Table 4-1: Suitability of various silicon lines for heating measurements

LINE	INTENSITY CHANGE WITH LASER FIRED	LINE IS ISOLATED	f,g, KNOWN
SiII - 4128 Å	DECREASES	NO	YES
SiII - 6347 Å	NONE	-	-
SiII - 5957 Å	DECREASES	YES	YES
SiII - 5056 Å	DECREASES	NO	YES
SiII - 5041 Å	DECREASES	NO	YES
SiII - 5979 Å	DECREASES	YES	YES
SiIII - 4553 Å	INCREASES	YES	YES

Figure 4-8: Line profiles of the SiIII line at 4553 Å and the SiII line at 5979 Å at various times after passage of the reflected shock

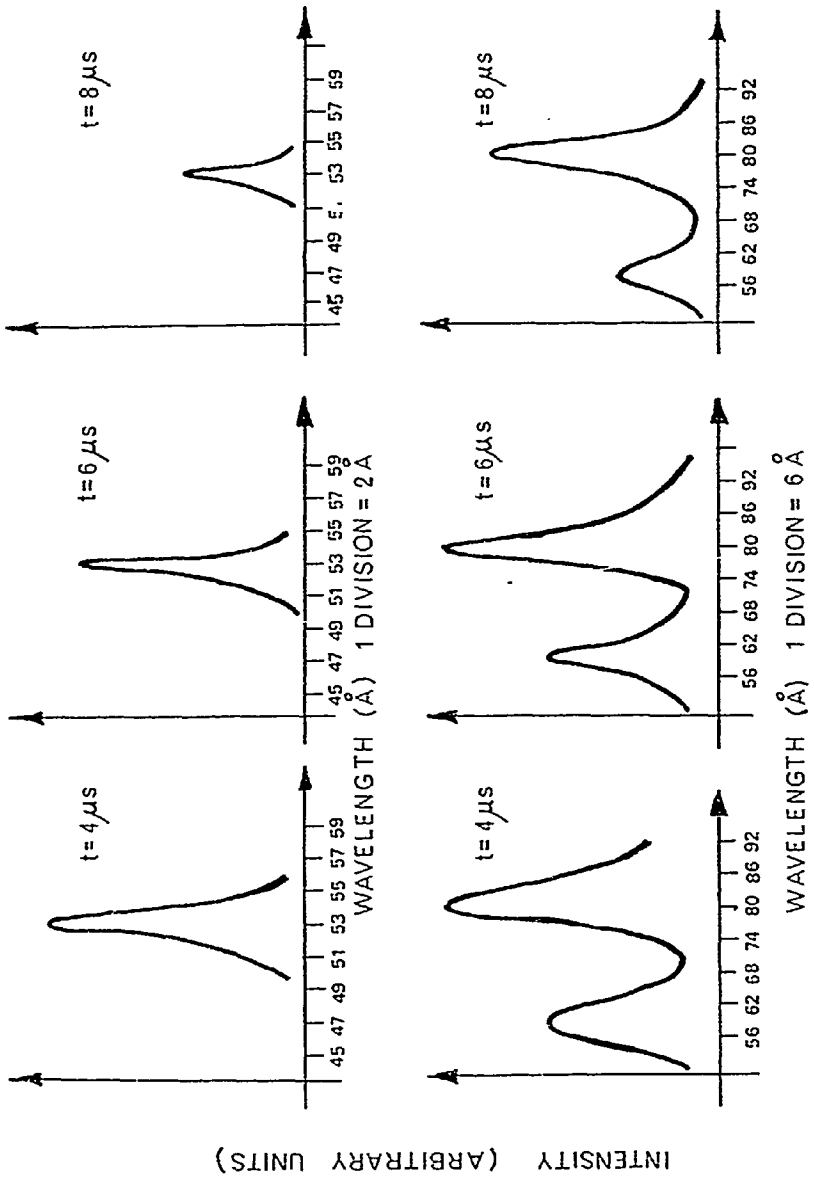
t=4μs
t=6μs
t=8μs
45 47 49 51 53 55 57 59
56 62 68 74 80 86 92
WAVELENGTH (Å) 1 DIVISION = 2 Å
WAVELENGTH (Å) 1 DIVISION = 6 Å
INTENSITY (ARBITRARY UNITS)
(a) Si III 4553 Å
(b) Si II 5979 Å

oscillator strengths and statistical weights of the two lines had to be known and the lines had to be fairly well isolated from other lines in the plasma spectrum. Further the line intensities had to be sinsitive to temperature change in the temperature range investigated and it was also necessary for the silicon ions to be in local thermal equilibrium with the electrons, otherwise the ratio of the intensities of spectral lines would not be a valid method of calculating plasma temperature. The question of the validity of local thermal equilibrium will be treated later.

Table 4-1 lists some of the most prominent silicon lines in the plasma and the relevant information for each line. From the table it can be seen that the SiII line at 5979 Å and the SiIII line at 4553 Å both appear to be suitable. The two lines are also quite well isolated from other lines as can be seen from Figure 4-8.

In order to measure the electron temperature T_e, it was necessary to know the ratio of the intensity of the SiIII line at 4553 Å to the intensity of the SiII line at 5979 Å as a function of temperature. In Chapter 2 it was shown that the ratio of the intensities of two lines from subsequent stages of ionization is given by

$$\frac{I'}{I} = \frac{f'g'\lambda^3}{fg\lambda'^3} \frac{1}{4\pi^{3/2}a_o^3 n_e} \left(\frac{T_e}{13.6}\right)^{3/2} \exp\left[-\frac{E'+E_\infty-E-\Delta E_\infty}{T_e}\right] \qquad (4\text{-}1)$$

where the meaning of the symbols is given in Chapter 2, part B and T_e is measured in eV.

For the SiIII line at 4553 Å the values of the quantities in equation (4-1) are [33]

Figure 4-9: Intensity ratio of the SiIII (4553 Å) line to the SiII (5979 Å) line as a function of temperature

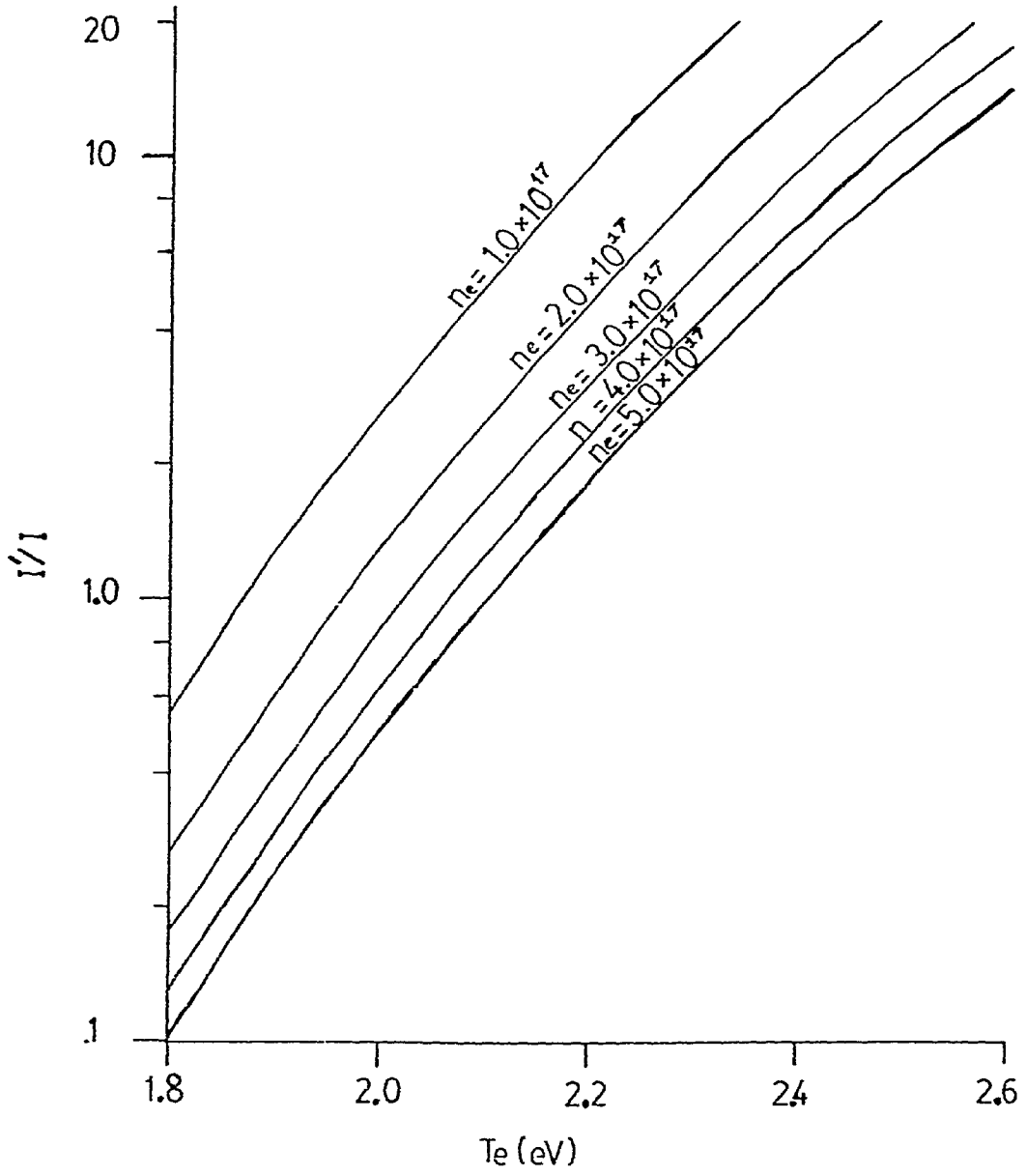
20
10
1.0
.1
I'/I
ne=1.0×10^17
ne=2.0×10^17
ne=3.0×10^17
ne=4.0×10^17
ne=5.0×10^17
1.8
2.0
2.2
2.4
2.6
Te (eV)

Figure 4-10: The electron temperature and density in the reflected shock at times measured after passage of the reflected shock

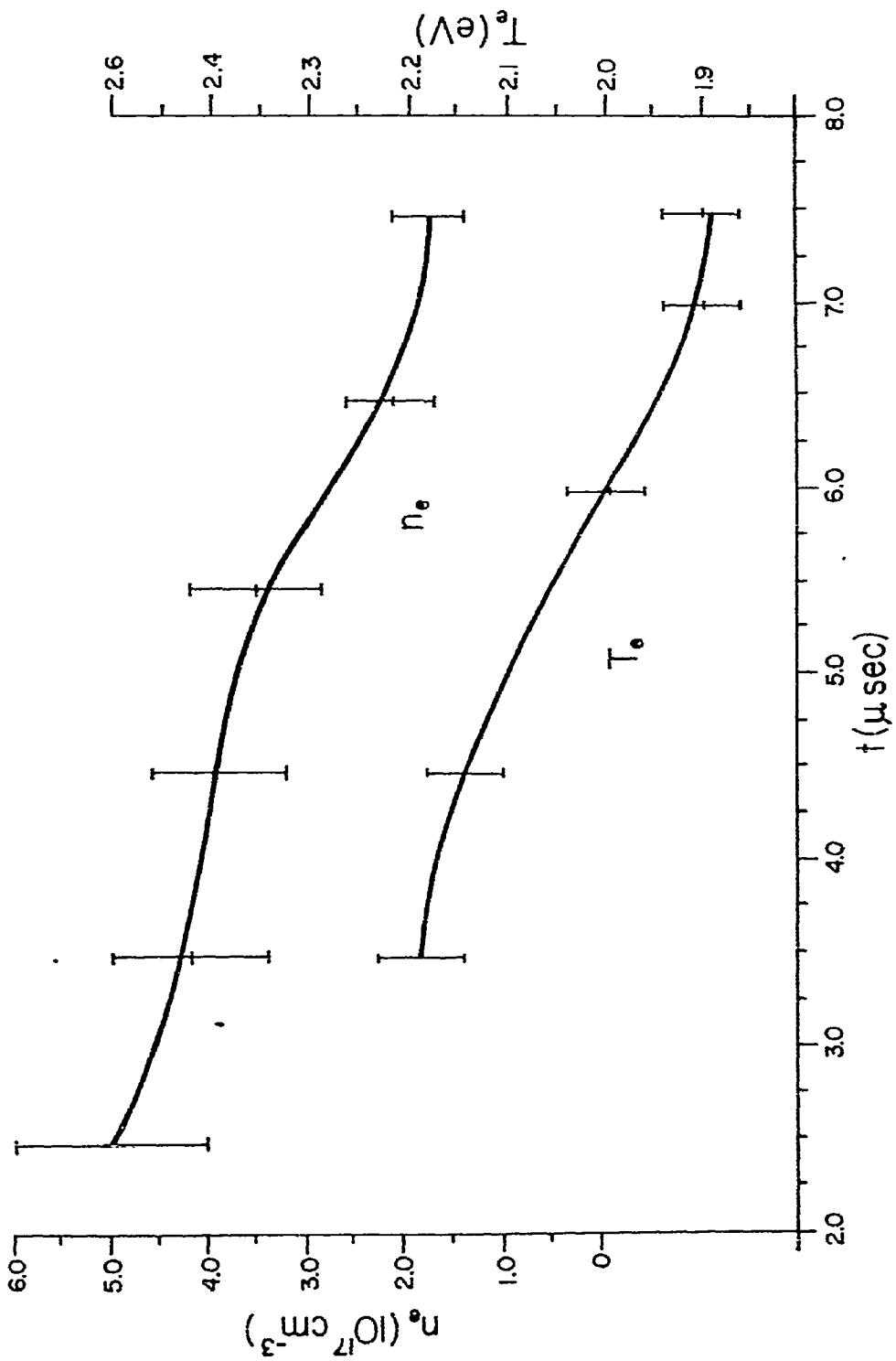
n_e (10^{17} cm^{-3})
6.0
5.0
4.0
3.0
2.0
1.0
0
T_e (eV)
2.6
2.4
2.3
2.2
2.1
2.0
1.9
n_e
T_e
2.0
3.0
4.0
5.0
6.0
7.0
8.0
t (μ sec)

$f' = 0.691$

$g' = 2J+1 = 2(1)+1 = 3$

$E' = 21.63eV$

For the SiII line at 5979 Å

$f = 0.215$

$g = 2J+1 = 2(3/2)+1 = 4$

$E = 12.09eV$

Also

$E_\infty = 16.34eV$

and

$\Delta E_\infty = 0.29eV$

Substituting these values in equation (4-1) gives

$$\frac{I'}{I} = \frac{3.3\times10^{22}}{n_e} T_e^{3/2} e^{-25.6/T_e} \qquad (4\text{-}2)$$

Figure 4-9 is a graph of I'/I as a function of T_e for a number of different values of n_e.

The total intensity of each silicon line was obtained in one shot by setting the monochromator so as to have a bandwidth of 10 Å which was large enough to include almost the entire line profile.

The electron density was again measured using the stark broadened half width of HeI (5876 Å)

The electron temperature and density for times greater than ~3.5 μs is shown in Figure 4-10. It is worth pointing out that the temperatures and densities at ~3 μs were measured using Si lines and He lines and the results were in good agreement.

Figure 4-11: Schematic diagram of set up used to measure temperature and density of plasma in the sidearm and to photograph the path of the laser in the plasma

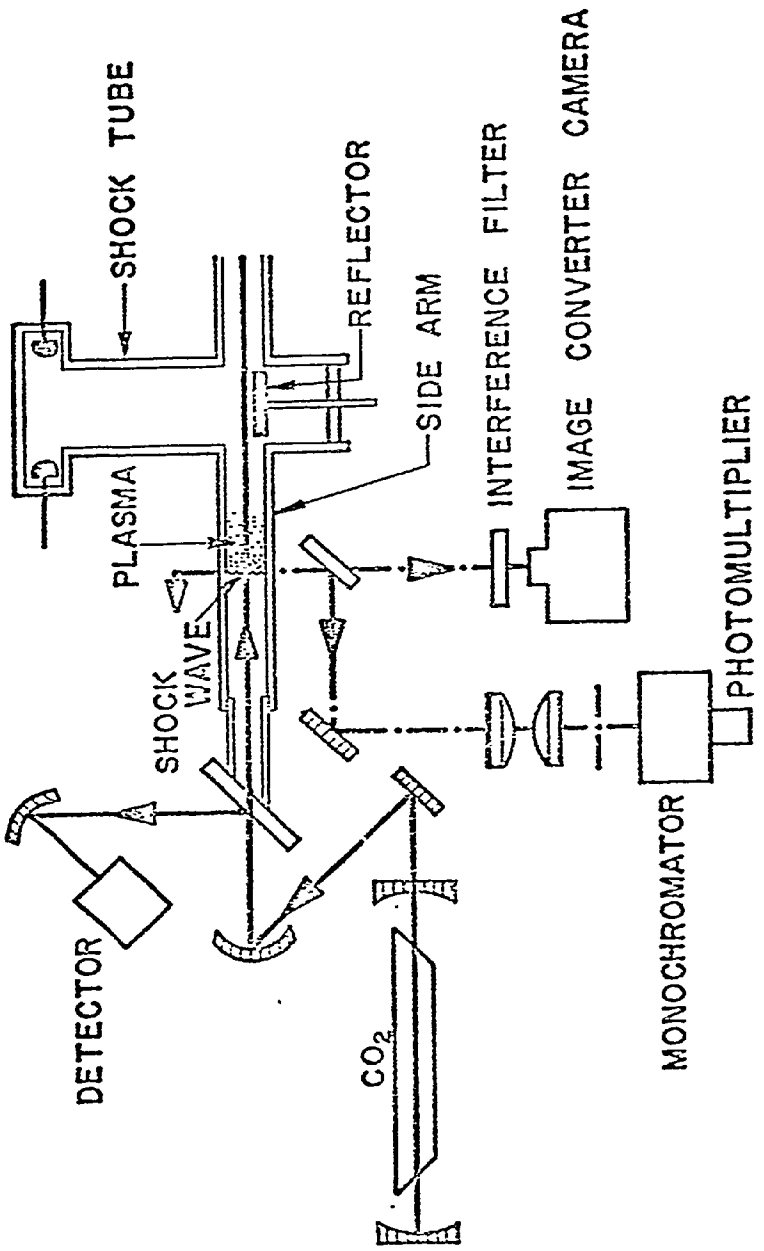
SHOCK TUBE
REFLECTOR
SIDE ARM
INTERFERENCE FILTER
IMAGE CONVERTER CAMERA
PLASMA
SHOCK WAVE
PHOTOMULTIPLIER
DETECTOR
CO_2
MONOCHROMATOR

Figure 4-12: Electron temperature and density in the sidearm plasma as a function of time

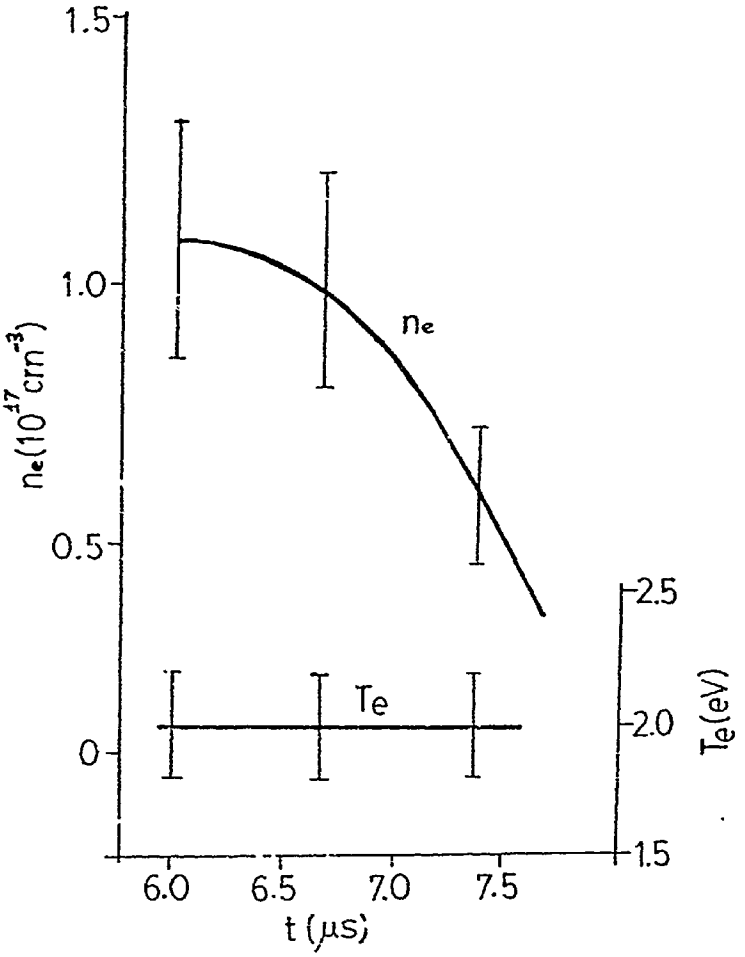
1.5
1.0
0.5
0
$n_e(10^{17}cm^{-3})$
n_e
T_e
2.5
2.0
1.5
$T_e(eV)$
6.0
6.5
7.0
7.5
t (μs)

Figure 4-13: Typical oscilloscope traces of silicon line signals and laser pulse: the dotted lines represent signal levels without laser (intensity increases in the negative direction)

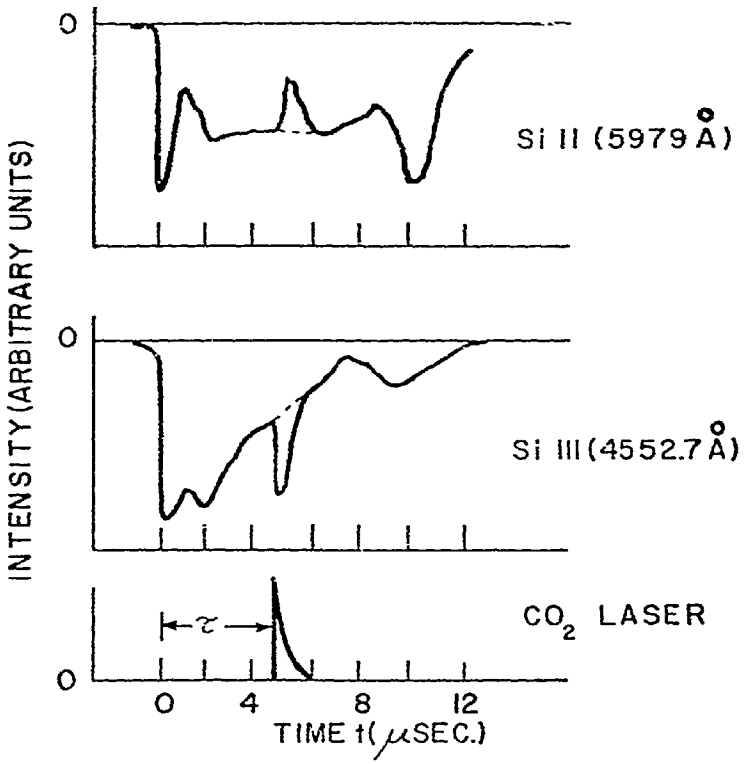
0
Si II (5979 Å)
0
Si III (4552.7 Å)
τ
CO_2 LASER
0
0
4
8
12
TIME t(μSEC.)
INTENSITY (ARBITRARY UNITS)

Fig. 2

Therefore combining Figure 4-7 and Figure 4-10 we have a continuous record of the temperature and density of the plasma from 0 μs to ~7.5 μs after passage of the reflected shock.

All of these measurements were made by 'looking' along the axis of the laser so the temperature and density are the average values of these quantities over the length of the plasma. The plasma has started to expand into the side arms after 3.5 μs. By setting the monochromator to look down on the sidearm from above as shown in Figure 4-11, the temperature and density in the sidearm at a distance of 6 cm from the main shock tube was recorded. The results of these measurements are shown in Figure 4-12.

In this section the electron temperatures and densities of the plasma were obtained spectroscopically, however, in order for the measurement of temperature by this method to be valid the plasma must be in local thermal equilibrium. Density measurements are independent of this requirement. The validity of local thermal equilibrium (LTE) for our plasma is discussed in the appendix.

4.5 Heating of the Plasma by the Laser

The laser was shot into the plasma at various times after reflection but no heating or change in spectral lines could be detected for times less than 3 μs. For times greater than 3 μs changes in the Si lines could be seen when the laser was fired into the plasma. The time delay between the plasma and the laser was varied to cover a wide range of absorption lengths.

Figure 4-13 shows typical photomultiplier signals of the line intensities of SiI and SiIII lines with the laser fired into the

Figure 4-14: Change in the intensity of the SiIII signal with the laser operating in the long pulse mode

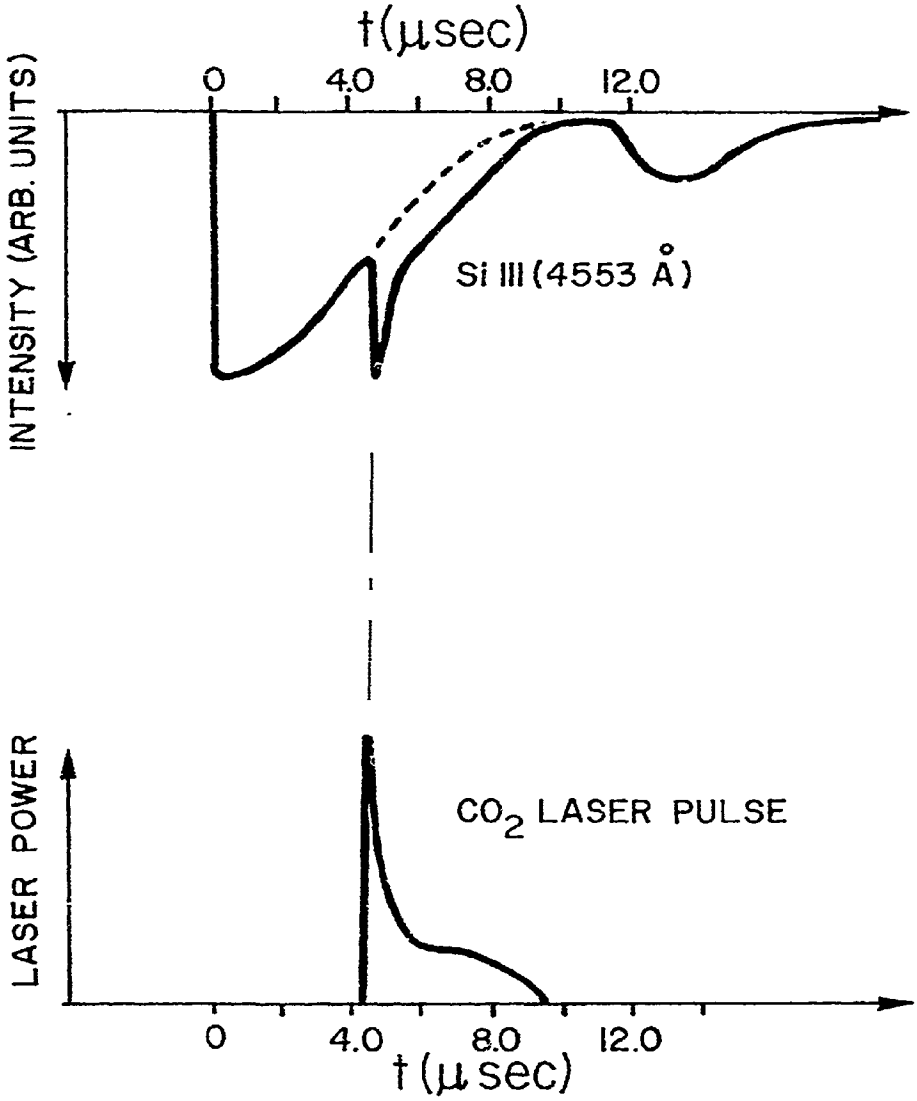
t(μsec)
0
4.0
8.0
12.0
INTENSITY (ARB. UNITS)
Si III (4553 Å)
LASER POWER
CO_2 LASER PULSE
0
4.0
8.0
12.0
t (μsec)

Figure 4-15: Intensity of the silicon lines as a function of time both with and without the laser: the primed quantities refer to SiIII

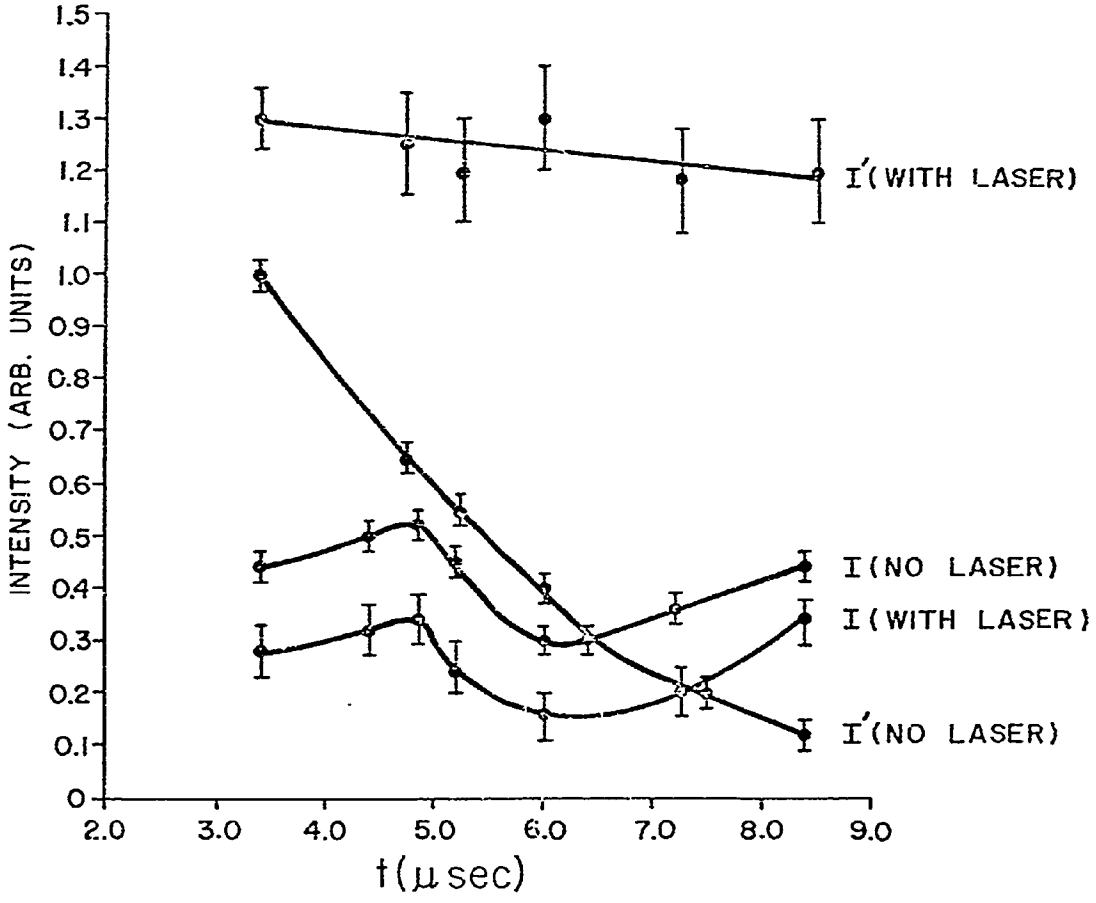
INTENSITY (ARB. UNITS)
1.5
1.4
1.3
1.2
1.1
1.0
0.9
0.8
0.7
0.6
0.5
0.4
0.3
0.2
0.1
0
2.0
3.0
4.0
5.0
6.0
7.0
8.0
9.0
t(μsec)
I'(WITH LASER)
I(NO LASER)
I(WITH LASER)
I'(NO LASER)

Figure 4-16: Electron temperature in the reflected plasma in the main shock tube before and after laser irradiation

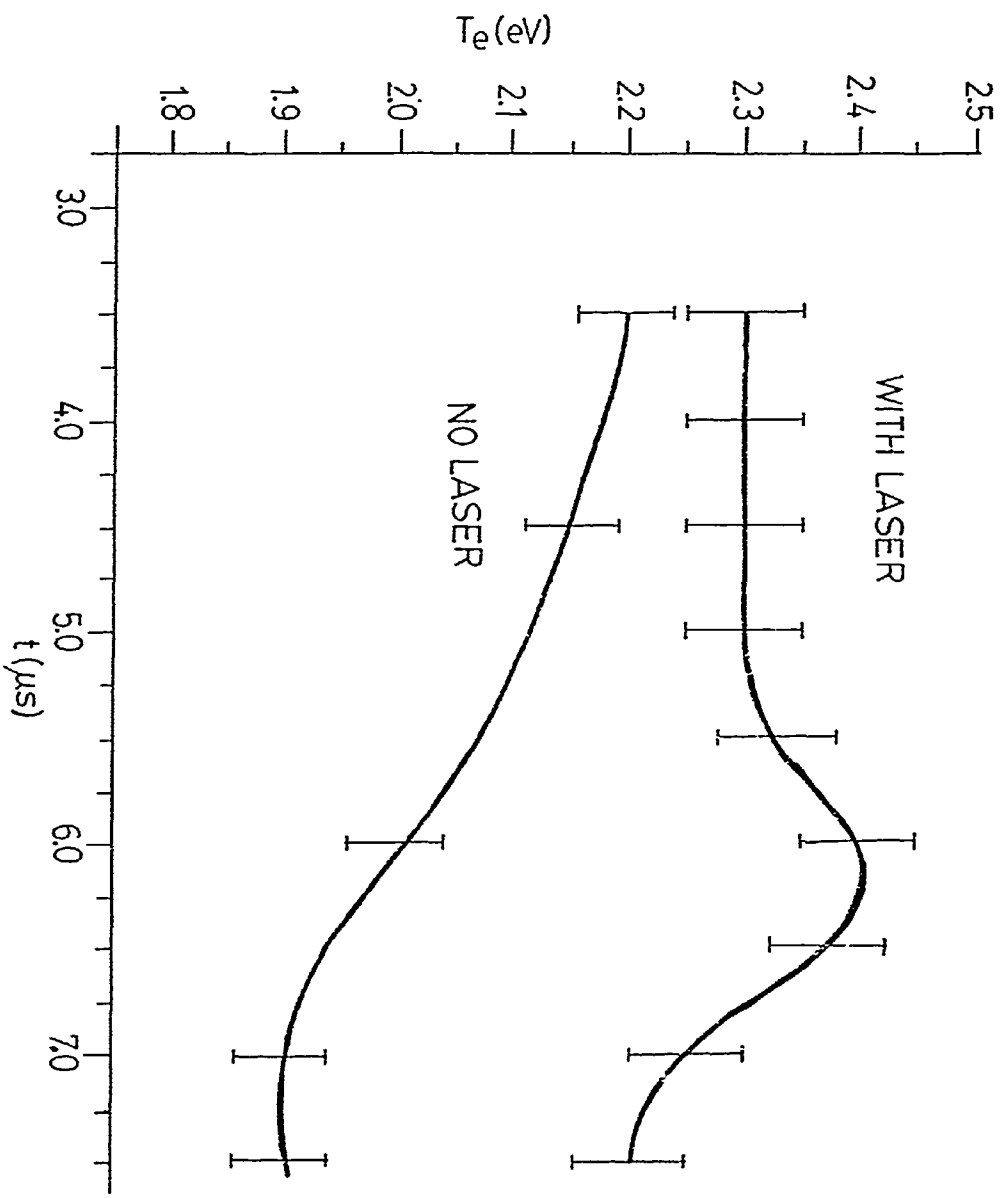
T_e(eV)
1.8
1.9
2.0
2.1
2.2
2.3
2.4
2.5
3.0
4.0
5.0
6.0
7.0
t (μs)
NO LASER
WITH LASER

plasma, the dotted lines showing the signal without the laser. An increase in the intensity of the SiIII radiation and a decrease in the intensity of the SiII radiation was observed for the duration of the laser pulse. This is what would be expected since an increase in temperature should increase the number of SiIII ions relative to the number of SiII ions. The rise time of the change in intensity was comparable to the rise time of the laser pulse. When a different gas mixture was used in the laser to obtain a different laser pulse shape the changes in the intensity of the Si lines approximately followed the laser intensity as shown in Figure 4-14.

Figure 4-15 shows the intensities of the two silicon lines as a function of time both with and without the laser. I' refers to the intensity of SiIII at 4553 Å and I refers to the intensity of the SiII line at 5979 Å. From the ratio of the intensities of the two lines a graph was made of the temperature of the plasma as a function of time both with and without the laser. The graph is shown in Figure 4-16. These results will be discussed in Chapter 5.

4.6 Photographic Observation of the Path of the Laser in the Plasma

Using the Saha and Boltzmann equations the intensity of the SiIII line at 4553 Å was calculated as a function of electron temperature and density. The results are shown in Figure 4-17. The intensity is very sensitive to temperature changes in the range from 2 to 5eV. In the range from 2.0 to 2.7eV the intensity of the line is not very sensitive to the electron density. Since the intensity was so sensitive to changes in temperature it was possible to observe a large increase in the intensity of the SiIII line when the laser was

Figure 4-17: Variation in the intensity of SiIII line (4553 Å) radiation with temperature and density for an LTE plasma

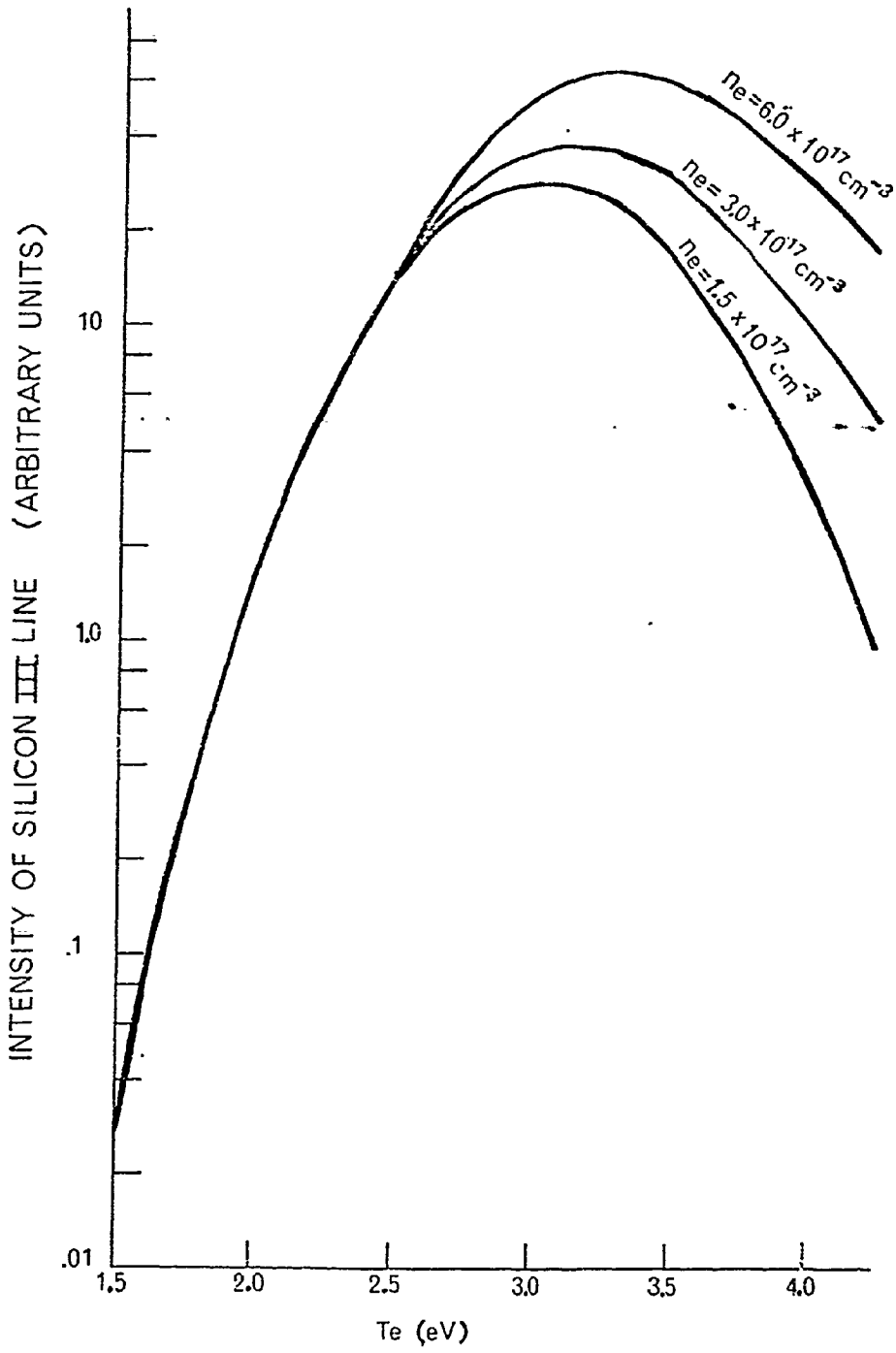
INTENSITY OF SILICON III LINE (ARBITRARY UNITS)
10
1.0
.1
.01
1.5
2.0
2.5
3.0
3.5
4.0
Te (eV)
ne=6.0 x 10^17 cm^-3
ne=3.0 x 10^17 cm^-3
ne=1.5 x 10^17 cm^-3

Figure 4-18: Image converter photographs of the reflected plasma using SiIII line radiation (a) with no laser (b) and (c) with laser beam, diameter 3 mm; (b) gap width 4 mm and beam centered at the gap; (c) gap width 7 mm and beam displaced with respect to the center of the gap, almost touching the reflector.

LASER
POSITION
(a)
(b)
REFLECTOR
(a)
(b)
(c)

shot into the plasma. The experimental apparatus was set up as shown in Figure 4-11. The image converter camera was set up to look at the plasma at right angles to the direction of propagation of the laser beam. The camera was used to photograph the plasma with an exposure time of 0.5 μs, both with and without the laser. An interference filter centered on the SiIII line at 4553 Å, with a bandwidth of 50 Å, was placed in front of the camera. Observations were made separately on the plasma in the main shock tube and on the plasma in the sidearm. From the increase in intensity it was possible to observe the length of the plasma column being heated. For times less than 4 μs after formation of the reflected shock no change in intensity due to the laser could be detected. At about 6 μs, the entire length of the plasma column appeared brighter and the entire width of the gap between the shock tube and the reflector showed increased brightness. In order to observe any possible lateral expansion of the plasma, the gap was increased from 4 mm to 7 mm. Figure 4-18 shows the photographs of the plasma with and without the laser. Figure 4-18(a) shows the plasma without the laser. Figure 4-18(b) shows the plasma with the shock tube-reflector gap set at 4 mm and the laser centered on the gap. Figure 4-18(c) shows the plasma with the gap set at 7 mm and the laser beam displaced with respect to the center of the gap, almost touching the reflector. It is seen that almost the whole region of plasma in the gap radiated much brighter when the laser was fired into the plasma, indicating that the laser heated plasma had a diameter much larger than the original diameter of the laser beam.

Figure 4-19: Image converter pictures of the plasma in the sidearm using SiIII line radiation; (a) without laser and (b) with laser; framing time 0.5 μs

(a)

(b)

The sharp boundary at the top of each photograph is due to the wall of the main shock tube.

Figure 4-19 shows the plasma in the sidearm. The plasma was moving to the left and the laser beam was propagating to the right. The picture shown in Figure 4-19 was taken ~6 μs after the formation of the reflected shock. Figure 4-19(a) shows the plasma with no laser and Figure 4-19(b) shows the plasma with the laser. The path of the laser beam can be seen as a thin bright filament.

CHAPTER 5: ANALYSIS OF THE EXPERIMENTAL RESULTS

5.1 Absorption Length and Temperature Changes

The absorption length of a plasma was shown in Chapter 2 to be

$$\ell = \frac{2.3 \times 10^{36} T_e^{3/2}}{n_e^2 \lambda^2}$$

Using the values of temperature and density from Figure 4-9 the absorption length of the plasma as a function of time was calculated and is shown in Figure 5-1. The absorption length ℓ appears to have two separate time constants. From 3.5 μs to 6 μs the change in the absorption length is very slow. After 6 μs the absorption length increases rapidly over the next 1.5 μs. In the first part of the graph ℓ increases from ~.2 cm to ~.6 cm. The absorption length in this region is much smaller than the length L of the plasma in the direction of the laser. L/ℓ is in the range 5 to 15. In the second stage ℓ increases rapidly reaching ~1/2 L.

Also shown in Figure 5-1 is $\Delta T_e/T_e$ as a function of time, ie. the fractional increases in the electron temperature due to laser heating as a function of time. During the time from 3.5 μs to ~6.5 μs

Figure 5-1: Absorption length ℓ of the plasma in the main shock tube before laser heating and the fractional increase in temperature $\Delta T/T$ due to the laser

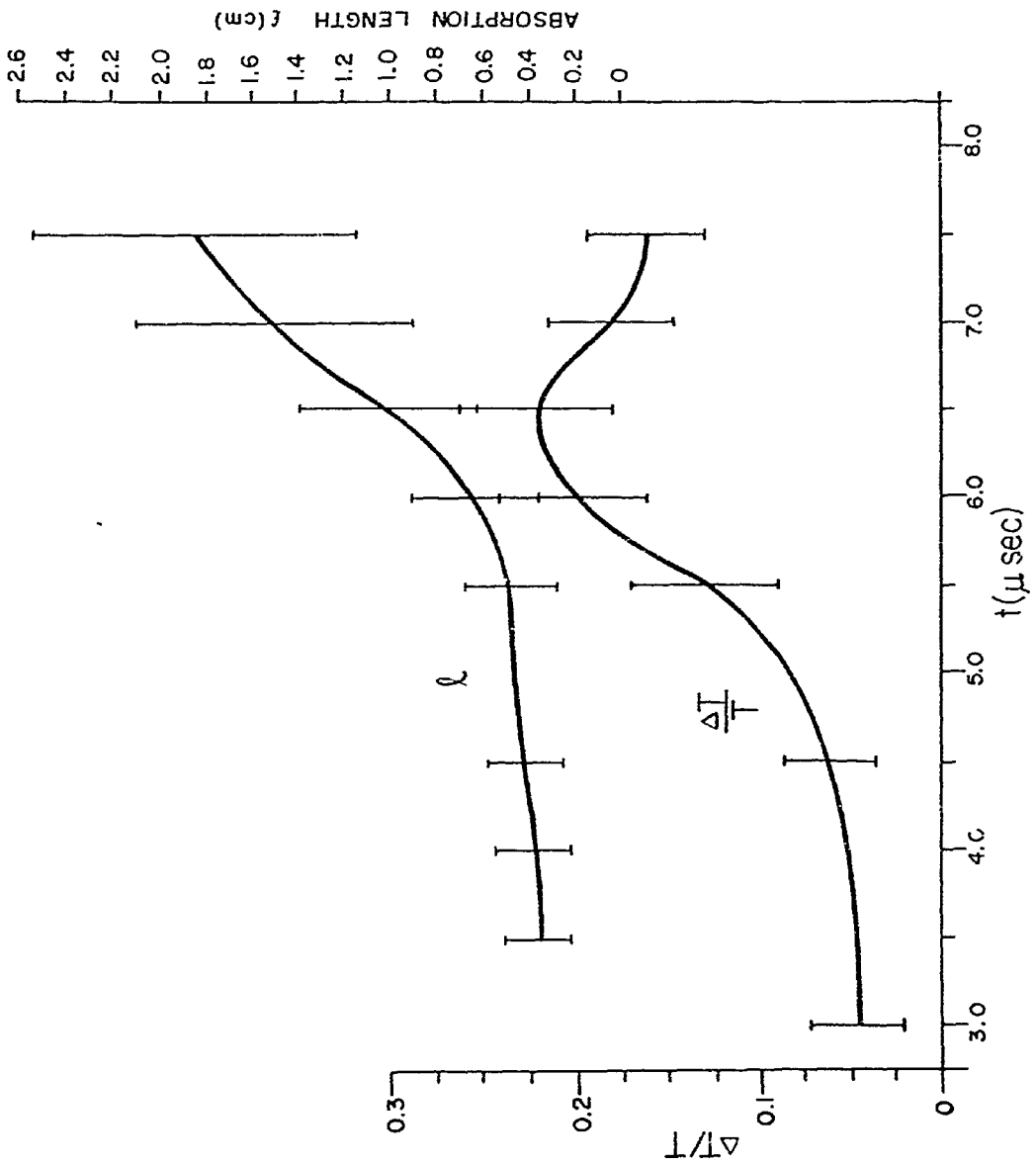
ABSORPTION LENGTH ℓ(cm)
2.6
2.4
2.2
2.0
1.8
1.6
1.4
1.2
1.0
0.8
0.6
0.4
0.2
0
ℓ
ΔT/T
0.3
0.2
0.1
0
3.0
4.0
5.0
6.0
7.0
8.0
t(μ sec)

the fractional change $\Delta T_e/T_e$ increases as the absorption length increases. After ~6.5 μs $\Delta T_e/T_e$ drops rapidly as would be expected since the plasma was becoming transparent to the laser radiation as can be seen from the graph of ℓ versus time. The measured maximum value of ΔT_e was 0.4eV for a plasma of initial temperature 2eV and density $3\times10^{17}cm^{-3}$ for which $L/\ell \approx 3$. It is quite possible that a much larger local increase in temperature may have resulted from laser heating when $L/\ell>>1$, ie. at earlier times, however the geometry of our detection system was such that it measured only the average increase in temperature over the whole plasma length. Therefore a large increase in T_e in a small region would have been masked by the much larger region of unheated plasma. This is consistent with image converter photographs of the plasma at early times which showed a short bright path of the laser beam at times ~2 μs.

5.2 Energy Necessary for Temperature Changes

As noted previously when the laser was fired into the plasma 6 μs after its formation the temperature of the plasma increased from 2.0 to 2.4eV. The absorption coefficient at this time was 1.6 $cm.^{-1}$ From image converter photographs the main shock tube plasma had a diameter of about 3 cm. If E_o is the incident laser energy then the amount of energy absorbed by the plasma was $E_o(1-e^{-\alpha L})$ where α is the absorption coefficient. For an incident energy of 0.3J the energy absorbed would be $.3(1-e^{-1.6(3)}) \approx .3J$. Therefore virtually all of the energy would have been absorbed and in fact no laser energy could be detected coming out of the plasma. If we assume that the heated

plasma was a cylinder of radius r = 1.5 mm (radius of the laser beam) and of length 3 cm then the amount of energy required to heat the plasma from 2.0eV to 2.4eV is given by

$$E = \frac{3}{2}(n_e+n_i)K(T_{ef}-T_{ei})\pi r^2 L \qquad (5\text{-}1)$$

where T_{ef} and T_{ei} are the final and initial electron temperatures respectively in Kelvins.

For the time 6 μs

$n_e = n_i = 3\times10^{17}cm^{-3}$

$T_{ef} = 2.4eV = 27840\ K$

$T_{ei} = 2.0eV = 23200\ K$

$L = 3\ cm$

$r = .15\ cm$

This gives E = .012 joules for the energy required to heat the plasma. Since this represents only ~4% of the incident laser energy there must be other energy sinks in the plasma.

5.3 Laser Energy Loss Mechanisms

5.3.1 Refraction of the Laser Beam

One possible source of energy loss may have been the refraction of the laser beam out of the plasma. The index of refraction μ of a plasma is given by

$$\mu = \left(1 - \frac{\nu_p^2}{\nu_\ell^2}\right)^{1/2} = \left(1 - \frac{n_e}{n_{ec}}\right)^{1/2} \qquad (5\text{-}2)$$

where ν_ℓ is the laser frequency, ν_p is the plasma frequency and n_{ec} is

the critical density, that is the density at which the plasma frequency equals the laser frequency. For a plasma with $n_e < n_{ec}$ the refractive index of the plasma is less than one and increases in regions of lower plasma density. Since light rays in an inhomogeneous region of a medium always bend towards the region of higher refractive index, the laser will be refracted towards regions of lower plasma density. If a plasma has a density profile which is maximum at the center and decreases towards the edge of the plasma then a laser beam will be refracted out of the plasma. If however the plasma has a minimum value of plasma density in the region in which the laser is propagating then the laser beam can be 'trapped' in the plasma. It is also possible for the laser to heat the plasma and form its own minimum density path through the plasma.

There is no reason why we would expect a large density gradient at the centre of the plasma through which the laser beam passed and experimentally we were not able to detect refraction of the laser beam by the plasma at times greater than 3 μs. The path of the laser through the plasma in the sidearm was photographed and as can be seen from Figure 4-19 the path was a straight line. The photographic evidence for the plasma near the reflector was not as good but faint burn marks on exposed Polaroid film produced when the laser passed through the plasma for times >3 μs showed no displacement from the position of the burn marks with no plasma. For these reasons refraction was not considered as an energy loss factor.

5.3.2 Laser Beam Reflection

The classical reflectivity of a plasma is given by

$$R = \left(\frac{\mu-1}{\mu+1}\right)^2 \qquad (5\text{-}3)$$

where τ is the refractive index of the plasma.

For a plasma of density $n_e = 3\times10^{17}cm^{-3}$ the reflectivity is only .02%. Even at a density of $10^{18}cm^{-3}$ the reflectivity is still less than .1% so obviously the classical reflection of the beam from the plasma is of no importance.

5.3.3 Laser Scattering

At high laser intensities it is possible to have stimulated Brillouin scattering and stimulated Raman scattering. These scattering processes are however, only important at very high laser intensities. The threshold intensity, I_B, for Brillouin scattering is given by [36]

$$I_B \sim 5\times10^{-15}\,\frac{n_e}{\lambda^2 T_e^{1/2}} \quad watts/m^2 \qquad (5\text{-}4)$$

The threshold intensity, I_R, for Raman scattering is given by [36]

$$I_R \sim \frac{10^{-24} n_e^{\,2}\lambda}{T_e^{1/2}} \quad watts/m^2 \qquad (5\text{-}5)$$

For our plasma these values are $I_B \sim 10^{14}$ watts/m^2 and $I_R \sim 7\times10^{17}$ watts/m^2. The intensity of the CO_2 laser used in this experiment in the plasma region was $\sim10^{12}$ watts/m^2 so neither of these

two processes should be of concern.

5.3.4 Thermal Conductivity of the Plasma

If heat is rapidly conducted away from the laser heated region it will of course be more difficult to obtain large increases in the plasma temperature. The thermal conductivity of a plasma can be represented by a characteristic length for conduction of heat, ie. if δ is the length in cm that heat will conduct in a time τ then [2]

$$\delta^2 = \frac{9.3\times10^{19} T_e^{5/2}}{(n_e + n_i)} \tau \qquad (5\text{-}6)$$

where T_e is in eV and n_e and n_i are in cm^{-3} and τ is in s.

Taking T_e = 2eV and $n_e = n_i = 3\times10^{17} cm^{-3}$ and taking τ to be the laser pulse length in s

$$\delta \approx .13 \text{ mm}$$

Taking the laser heated region to be ~3 mm in diameter it can be seen that δ<< diameter of the laser heated region so heat loss by conduction can be neglected.

5.3.5 Radiation Losses Due to Bremsstrahlung

According to Spitzer [34] the total amount of energy radiated in free-free transitions per cm^3 per second is given by

$$P_{ff} \approx 1.42\times10^{-34} n_e^2 T_e^{1/2} Z \text{ J/cm}^3\text{/s} \qquad (5\text{-}7)$$

where Z = 1 for singly ionized helium and T_e is in Kelvins.

In our case for $n_e = 3 \times 10^{17} cm^{-3}$

and $T_e = 2eV = 23200\ K$

$P_{ff} \approx 2000\ J/cm^3/s$

Therefore during the heating time of 2×10^{-7}s the amount of energy radiated as bremsstrahlung was $\sim 4 \times 10^{-4}$ joules/cm^3. This energy is very small compared to the energy in the laser pulse, so bremsstrahlung radiation is unimportant.

5.3.6 Losses Due to Recombination Radiation

Recombination radiation or free-bound radiation, results when electrons undergo a transition from a free state to a bound state.

According to Griem [33], free-bound radiation is larger than free-free radiation by a factor $\frac{E_\infty}{T_e}$ where E_∞ is the ionization energy of the ion or atom. For helium the ionization energy is 24.48eV so for the case when $T_e = 2eV$, $P_{fb} \sim 25000\ J/cm^3/s$. Therefore the energy lost due to free-bound transitions is $\sim .005\ J/cm^3$ which is still small enough to ignore.

5.3.7 Line Radiation Due to Impurities

Line radiation due to impurities in the plasma can quite often be large but it is difficult to estimate the loss unless the percentage of impurities is known.

As an example consider the SiIII ion. According to Griem [33] almost all of the energy emitted as line radiation is due to the resonance line and all other lines for that ionization stage may be neglected. The power emitted in the resonance line of an impurity of

density n_a, where E_a is the excitation energy of the resonance line is given by [33]

$$P_{line} = 6.65\times10^{-6} n_a \exp(-\frac{E_a}{T_e}) \text{ watts/cm}^3 \qquad (5-8)$$

For SiIII this results in a power of $\sim 4.5\times10^{-10} n_a$ watts/cm^3. The energy lost during the time of heating would be $\sim 9\times10^{-17} n_a$ joules/cm^3. For a 1% SiIII impurity $n_a = 3\times10^{15}$, the energy loss would be 0.27 joules/cm^3. This represents a sizeable energy loss however as was pointed out in the appendix the plasma is optically thick for the resonance line if $n_a \gtrsim 1.4\times10^{13}\text{cm}^{-3}$. Therefore we can conclude that either the SiIII resonance line is trapped in the plasma or the SiIII concentration is low enough ($<1.4\times10^{13}\text{cm}^{-3}$) so that the energy loss would be negligible.

5.3.8 Plasma Expansion

Expansion of the plasma becomes important when the heating time τ is greater than or comparable to the time required for an acoustic wave to traverse the region of the plasma which has been heated.

The velocity of an acoustic wave in a plasma is given by [34]

$$v_s = \left[\frac{(Z+1)\gamma KT_e}{M}\right]^{\frac{1}{2}} \qquad (5-9)$$

where Z = 1 for singly ionized helium

γ is the ratio of the specific heats

T_e is in Kelvins

and M is the mass of the helium ion in kg.

Figure 5-2: Schematic diagram of cylindrical section of the plasma through which the laser passes; r_o is the original radius and r is the radius after expansion

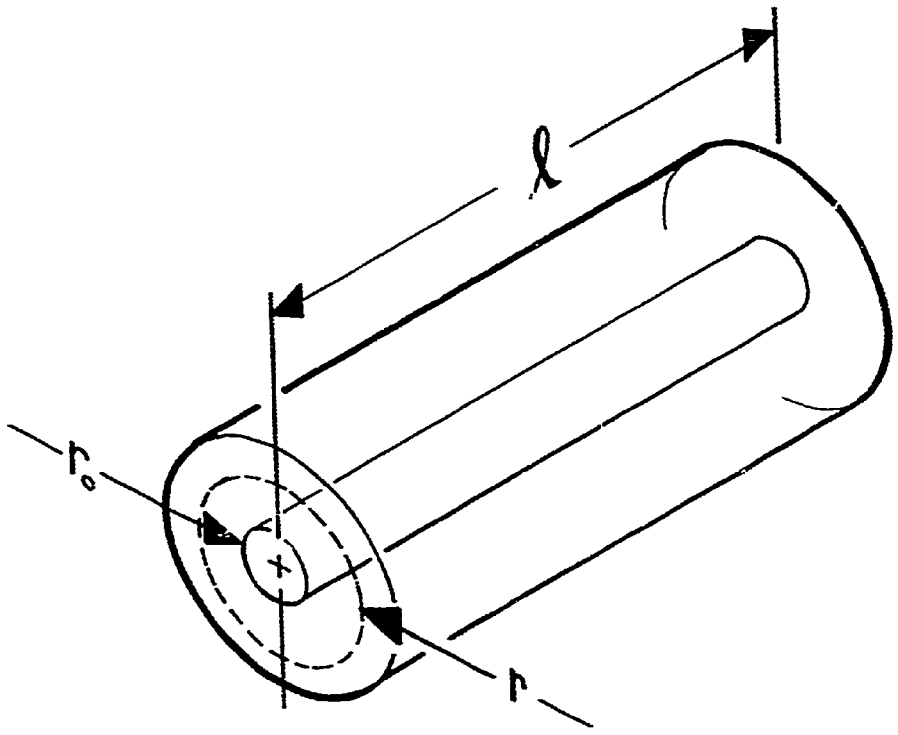
l
r_o
r

From equation (5-9) the velocity of an acoustic wave in our case was $v_s = 1.3 \times 10^5$ cm/s. The diameter of the heated region of the plasma was ~3 mm so the time required for an acoustic wave to travel this distance was ~230 ns. Since this time is about the same as the heating time (200 ns) expansion must be considered to be an important factor in determining where the absorbed laser energy has gone.

5.4 Expansion of the Plasma

As discussed in the previous section the laser energy absorbed by the plasma appeared to go predominantly into increasing the plasma temperature and into expansion of the plasma. In this section a calculation of the expansion will be made.

The electron-ion thermalization time is given by [34]

$$t_{ie} = \frac{3.32 \times 10^{6} A T_e^{3/2}}{n_e Z \ln\Lambda} \qquad (5\text{-}10)$$

where $\ln\Lambda \approx 5$, A the atomic weight = 4, Z = 1 for singly ionized He and T_e is measured in eV.

For our case this gives $t_{ie} \approx 2.5$ ns. Since $t_{ie} <<$ the heating time τ the electrons and ions both have the same temperature, T.

We also assume that there is no further ionization caused by the laser. The basis for this assumption was that no change in the electron density could be detected when the laser was shot into the plasma.

Letting E be the initial energy in the laser pulse, the amount of energy absorbed by the plasma with an absorption coefficient α and length L would be

$$E(1-e^{-\alpha L})$$

The work done in expansion from an initial volume V_o to a final volume V_f is

$$\int_{V_o}^{V_f} pdV$$

where p is the plasma pressure and

$$p = (n_e+n_i)KT$$

For a cylindrical plasma of length L and radius r the volume $V = \pi r^2 L$. Therefore the work done in expansion is

$$W = \int_{r_o}^{r} (n_e+n_i)KTdV \quad \text{where } r_o \text{ is the original radius.}$$

For a singly ionized plasma $n_e = n_i$

Assuming expansion into a plasma at a constant temperature

$$W = \int_{r_o}^{r} 4\pi L n_e KTrdr$$

$$W = 2\pi L n_e KT[r^2-r_o^2]$$

$$= 1.8[r^2-2.25\times10^{-2}] \text{ joules}$$

The energy going into heating is

$$\frac{3}{2}\int_{T_i}^{T_f} KV(n_e+n_i)dT$$

where T_i and T_f are the initial and final temperatures respectively.

The equation for the energy balance in the plasma is

$$E[1-e^{-\alpha L}] = \int_{V_o}^{V_f} pdV + \frac{3}{2}\int_{T_i}^{T_f} KV(n_e+n_i)dT \qquad (5\text{-}11)$$

Measurements of the temperature and density of the plasma in the sidearm plasma indicate that it would have absorbed about 70 mJ of the 300 mJ of energy in the laser beam. Therefore 230 mJ would have been incident on the plasma between the shock tube and the reflector. The initial temperature of the plasma was 2.0eV and the final temperature was 2.4eV. The electron density $n_e = 3\times10^{17}cm^{-3}$. Taking the initial radius of the heated plasma to be 1.5 mm we can use equation (5-11) to calculate a value for the final radius of the heated plasma. Equation (5-11) becomes

$$0.23 = 1.8[r^2-2.25\times10^{-2}] + 0.54r^2$$

Solving for r gives r = 3.4 mm as the final radius of the heated plasma. Such a large expansion is consistent with the image converter photographs for the 7 mm gap shown in Figure 4-18(c).

The average expansion velocity of the plasma from r_o = 1.5 mm to r = 3.4 mm assuming an expansion time equal to the duration of the laser pulse was 1.1×10^6cm/s which is approximately equal to the

velocity of an acoustic wave in the plasma which was 1.3×10^6cm/s.

Evaluating the two terms on the right of equation 5-11 the energy which went into plasma expansion was 0.17 joules and the energy which went into heating was 0.06 joules or ~70% and ~30% respectively.

5.5 Conclusions and Suggestions for Further Research

In conclusion we were able to heat a low temperature, high density plasma from 2.0eV to 2.4eV with a high power CO_2 laser. It was found that ~30% of the laser beam energy went into temperature increase while ~70% went into plasma expansion. It was pointed out that much larger temperature increases may have occurred but since we only measured the average temperature over a large length of plasma, large local temperature changes may have occurred but not been detected. This problem would have been overcome by using a method of temperature measurement that gives a high spatial resolution such as laser scattering.

It was noted earlier that no plasma heating could be observed when the laser was fired into the incident shock. This was possibly due to the fact that the plasma behind the incident shock wave was moving so that the heated plasma would have moved out of the observation region. The plasma behind the incident shock wave also had a density gradient in direction of propagation of the shock wave which could have reflected the laser beam out of the plasma. This problem could be reduced by shooting the laser into the plasma parallel to the direction in which the plasma was moving. The density gradients encountered by the laser in this case would be less. This

idea is supported by observation of the laser striking the plasma in the sidearm plasma as shown in Figure 4-19. From the photograph it can be seen that the laser was not deflected.

In order to increase the amount of plasma heating a number of steps could be taken. The density of the plasma could be increased, although not by too much since the critical density for CO_2 laser beam reflection is $10^{19}cm^{-3}$. A magnetic field could be used to try to confine the plasma and reduce the expansion of the plasma. Since in our experiment ~70% of the laser energy went into plasma expansion, reducing expansion could greatly increase the laser heating.

Greater laser power would also help and it would be especially interesting to increase the power to the point at which the anomalous absorption mechanisms become important.

APPENDIX

VALIDITY OF LOCAL THERMAL EQUILIBRIUM

A plasma is said to be in complete thermal equilibrium if the following conditions are satisfied:

(1) The radiation in the plasma can be described by the Planck function given below

$$B(\lambda,T) = \frac{2hc^2}{\lambda^5} \frac{1}{e^{hc/\lambda KT}-1} \qquad \text{(A-1)}$$

where T is the temperature of all species of particles and is the wavelength of the radiation.

(2) The particles in the plasma have a Maxwellian velocity distribution given by

$$dn_v = 4\pi n_e \left(\frac{m}{2\pi KT}\right)^{3/2} \exp\left(-\frac{mv^2}{2KT}\right) v^2 dv \qquad \text{(A-2)}$$

where n_e is the electron density and m is the particle mass.

(3) The distribution of population densities among the excited levels of the ions is given by boltzmann's equation.

$$\frac{n_n}{n_m} = \frac{g_n}{g_m} \exp\left[\frac{E_m - E_n}{KT}\right] \tag{A-3}$$

where E_n and E_m are the excitation energies of the two levels and g_n and g_m are the statistical weights of the two levels.

(4) The population densities of the various stages of ionization in the plasma are given by Saha's equation which can be written as

$$\frac{n_e n^z}{n^{z-1}} = \frac{Z^z}{Z^{z-1}} \left(\frac{mKT}{2\pi\hbar^2}\right)^{3/2} \exp\left[-\frac{E_\infty^{z-1} - \Delta E_\infty^{z-1}}{KT}\right] \tag{A-4}$$

where n^z and n^{z-1} are the densities of ions in two subsequent stages of ionization and E^{z-1} is the ionization energy of stage $z-1$ and E^{z-1} is a correction due to plasma interactions.[33]

If all four of the above equations hold then the plasma is in complete thermal equilibrium. In particular equation (A-1) is never satisfied. Conditions (2) (3) and (4) are often satisfied in laboratory plasmas so the name local thermal equilibrium was invented to describe plasmas which satisfy conditions (2) through (4).

LTE can be expected to hold if collisional processes with electrons from a Maxwellian destribution dominate the rate equations. That is, all atomic and ionic levels are populated and depopulated by electron collisions and radiative decay can be neglected.

Collision cross sections decrease with increasing temperature and

increase with higher densities. Also collision cross sections increase rapidly with principal quantum number n whereas radiative decay rates decrease. Therefore LTE would be expected to break down first at high temperatures, low densities and low values of the principal quantum number. Time variations and spacial inhomogeneities may further restrict the validity of LTE.

In order for equations (A-2) to (A-4) to be satisfied and the plasma be in LTE a number of conditions, discussed below, must be met.

(i) Self Collision Time

As electrons dominate the collision rates that determine the distribution among states described by the Saha and Boltzmann equations, it is necessary that the electrons have a Maxwellian velocity distribution as given by (A-2). Therefore the self collision time for electrons must be short compared to the time required for an electron to gain an energy of KT_e from an external source. The self collision time for electrons is given by [34]

$$t_c = \frac{2.66\times10^{-1}}{n_e \ln\Lambda} T_e^{3/2} \qquad \text{(A-5)}$$

where T_e is in Kelvins.

Therefore when $n_e = 3\times10^{17}\text{cm}^{-3}$

and $T_e = 23200$ K (2eV)

then $t_c = 6.3\times10^{-13}$s

This time is very much shorter than the time during which the laser is heating the plasma so the electrons should have a Maxwellian velocity distribution.

(ii) Density Requirement

By requiring that the collisional transition rate be ~10 times greater than the radiative decay rate, the criterion for complete LTE is given by McWhirter [35] to be

$$n_e \geq 1.6\times10^{12} T_e^{1/2} \chi^3 cm^{-3} \qquad (A-6)$$

with T_e in Kelvins and χ the energy of the resonance line in eV.

At times < 3.5 μs, the ratio of the intensities of HeII (4686 Å) to HeI (5876 Å) was used for temperature measurements so LTE must exist for HeI and HeII in order to get correct values for the temperature.

The energy of the resonance line for HeI is 21.3eV and for HeII the resonance line energy is 40.9eV. If the plasma is in LTE for HeII it will also be in LTE for HeI so applying equation (A-6) for a temperature of 3.5eV = 40600 K we have $n_e \geq 2.2\times10^{19} cm^{-3}$.

This is much higher than the density of our plasma but this criterion can be relaxed by about a factor of 10 if the plasma is optically thick for the resonance line. This is true if [33]

$$n_a d \geq \frac{1.1\times10^{17}}{f\lambda} \left(\frac{T_e}{A}\right)^{1/2} \qquad (A-7)$$

where n_a is the ion density in the ionization stage of the atom from which the line originates and T_e is in eV.

A is the atomic mass number

f is the absorption oscillator strength

λ is in Å

and d is a characteristic plasma dimension

For the HeII resonance line at 304 Å f = 0.4. Therefore $n_a d \geq 8.5 \times 10^{14} cm^2$. For d ~ 1 cm $n_a \geq 8.5 \times 10^{14} cm^{-3}$.

This is easily satisfied so we can relax the density requirement for LTE to $n_e \geq 2.2 \times 10^{18} cm^{-3}$. Although this condition isn't satisfied, equation (A-6) is only approximate and n_e is almost this large. According to McLean [28] working with a similar plasma, even though the plasma may not be in complete LTE it is close enough that the ratios of line intensities give temperatures accurate to within 15%.

At later times, t > 3.5 μs when the silicon lines were used to measure temperature the density n_e was 3×10^{17} and the temperature was 2eV. The resonance line for SiIII has an energy of 10.3eV and has an oscillator strength of 1.7. Therefore using equation (A-6)

$$n_e \geq 2.7 \times 10^{17} cm^{-3}$$

The condition for optical thickness for the resonance line becomes $n_a \geq 1.4 \times 10^{13} cm^{-3}$.

The density of SiIII is very likely higher than this so the density requirement can be reduced to $n_e \geq 2.7 \times 10^{16} cm^{-3}$. Since $n_e \approx 3 \times 10^{17} cm^{-3}$ the plasma should be in LTE as far as the SiIII is concerned.

(iii) Partial Local Thermal Equilibrium

As mentioned previously LTE breaks down first for low values of the principal quantum number n. It is possible to have the energy levels of highly excited states populated according to Boltzmann's equation even though the lower levels are not. If LTE holds for $n \geq 3$ for example, then the plasma is said to be in partial LTE.

According to Griem [33] the electron density required for partial LTE is given by

$$n_e \geq \frac{7\times10^{18}Z^6}{n^{17/2}} \left(\frac{T_e}{13.6}\right)^{1/2} cm^{-3} \qquad \text{(A-8)}$$

where n is the principal quantum number of the lowest level included in the partial LTE

T_e is in eV

and Z = 1 for neutrals, 2 for singly ionized ions, etc.

(a) Helium Lines

The line 5876 $\mathring{A}$ of HeI involves the level n = 2. For HeI Z = 1 and taking T_e = 3.5eV we get $n_e \geq 9.8\times10^{15}cm^{-3}$.

The HeII line at 4686 $\mathring{A}$ involves the n = 3 level so in this case Z = 2 and $n_e \geq 2\times10^{16}cm^{-3}$. Therefore the plasma is in partial LTE according to the levels involving the lines used in this experiment.

(b) Silicon Lines

When the silicon lines were used the electron temperature was ~2eV and the density was $\sim3\times10^{17}cm^{-3}$.

The electronic structure of Si is $1s^2 2s^2 2p^6 3s^2 3p^2$. The transition responsible for the SiII line at 5979 $\mathring{A}$ is $3s^2 4p - 3s^2(^1s)5s$. The transition for the SiIII line at 4553 $\mathring{A}$ is $3s4s - 3s(^2s)4p$. Therefore in both cases the lowest quantum level involved is n = 4. For SiII partial LTE holds for $n \geq 4$ when $n_e \geq 1.3\times10^{15}cm^{-3}$. For SiIII partial LTE holds for $n \geq 4$ when $n_e \geq 1.5\times10^{16}cm^{-3}$. Both of these densities are small compared to the actual density so the plasma should be in partial LTE for $n \geq 4$.

(iv) Transient Plasmas

If a plasma, initially in LTE undergoes a change in electron temperature or density a certain time is required to reestablish LTE. The equilibration time for complete LTE is given by [33]

$$\tau = \frac{1.1\times10^{7} n_i^{z} T_e^{1/2}}{f n_e (n_i^{z-1}+n_i^{z})(13.6)^{3/2}} \exp(\frac{\chi}{T}) \text{ s} \qquad \text{(A-9)}$$

where n_i^{z} is the ion density in a particular ionization state

χ is the energy of the resonance line in eV

For T_e = 2eV and $n_e = 3\times10^{17}$ and for SiII and SiIII

$$\tau \approx (\frac{n_i^{z}}{n_i^{z}+n_i^{z-1}}).10^{-9} \text{ s}$$

Therefore the maximum value of $\tau \sim 10^{-9}$ s which is short compared to times of interest in our experiment.

The equilibration time for LTE for levels above the principal quantum number n is given by [33]

$$\tau_n^{z-1} \approx \frac{4.5\times10^{7} Z^2}{n^4 n_e} (\frac{T_e}{13.6})^{1/2} \exp(\frac{27.2Z^2}{n^3 T_e}) \text{ s} \qquad \text{(A-10)}$$

For the SiII ion and n = 4 with T_e = 2eV and $n_e = 3\times10^{17}\text{cm}^{-3}$

$\tau_4^{1} = 4\times10^{-13}$ s

and for the SiIII ion and n = 4

$\tau_4^{2} \approx 2\times10^{-12}$ s

These times are also very short compared to any time characteristic of a temperature or density change in the plasma.

It is worth noting that on laser radiation the rise time of the Si

line signals were observed to be approximately the same as that of the laser pulse thus confirming that the relaxation times were short compared to the laser pulse width. Thus the plasma is in LTE for the chosen Si lines and the corresponding spectral measurements give the plasma electron temperature.

REFERENCES

1. Chen, F.F., Introduction to Plasma Physics, Plenum Press, New York (1974).

2. Dawson, J.M., Princeton Plasma Physics Laboratory Report; MATT-786 (June 1970).

3. Dawson, J.M., Kidder, R.E., Hertzberg, A., Princeton Plasma Physics Laboratory Report; MATT-782 (Sept. 1971).

4. Basov, N.G., Krok-in, O.N., Soviet Physics Jetp 19 (1964) 123.

5. Kaw, P., Dawson, J.M., Phys. Fluids 12 (1969) 2586.

6. Kruer, W.L., Kaw, P.K., Dawson, J.M., Oberman, C., Phys. Rev. Letters, 24 (1970) 987.

7. Dawson, J.M., Oberman, C., Phys. Fluids 5 (1962) 517.

8. Johnston, T.W., Dawson, J.M., Phys. Fluids, 16 (1973) 722.

9. Engelhardt, A.G., Fucks, V., Neufeld, C.R., Richard, C., DeCoste, R., Appl. Phys. Letters, 20 (1972) 425.

10. DeCoste, R., Engelhardt, A.G., Fucks, V., Neufeld, C.R., J. of Appl. Phys., 45 (1974) 1127.

11. Molen, G.M., Kristianson, M., Hagler, M.O., App. Phys. Lett. 24 (1974) 583.

12. Box, S.J.C., Byszewski, W.W., John, P.K., Proceedings of the Twelfth International Conference on Phenominon in Ionized Gases Part 1, Eindhoven Aug. 1975.

13. Box, S.J.C., John, P.K., Byzewski, W.W., J. of Appl. Phys. 48 (1977) 1946.

14. Byzewski, W.W., Box, S.J.C., John, P.K., Plasma Physics and Controlled Nuclear Fusion Research, II, (1976) 627.

15. Kristiansen, M., Hagler, M.O., Nuclear Fusion 16 (1976) 999.

16. Schever, P.A.G., Monthly Notices Roy. Astron. Soc., 120, 231 (1960).

17. Tanenbaum, B.S., Plasma Physics, McGraw-Hill (1967).

18. Ginsburg, V.L., The Propagation of Electromagnetic Waves in Plasmas, Pergamon Press, Ltd., Oxford, 1964.

19. Hora, Heinrich, Physics of Fluids, 12 182 (1969).

20. Kaw, P.K., Dawson, J.M., Phys. of Fluids, 12 (1969) 2586.

21. DuBois, D.F., Goldman, M.V., Phys. Rev. Letters, 14, 544 (1965); Phys. Rev. 164, 207 (1967)

22. Jackson, E.A., Phys. Rev. 153, 235 (1967).

23. Beaulieu, A.J., Applied Phys. Letters, 16, 504 (1970).

24. Fowler, Goldstein and Clotfelder, Phys. Rev., 82, 879 (1951).

25. Fowler, Atkinson, Marks, Phys. Rev., 87, 966 (1952).

26. Kolb, A.C., Phys. Rev., 107, 345 (1957).

27. McLean, E.A., Faneuff, C.E., Kolb, A.C., Phys. of Fluids, 3, 843 (1960).

28. Lie, Rhee, McLean, Phys. of Fluids, 13, 2492 (1970).

29. Bradley, John, Shockwaves in Chemistry and Physics, Wiley (1962).

30. Fucks, W., Theenhaus, R., Plasma Phys. 7 177 (1965).

31. Gibson, A.F., Kimmitt, M.F., Walker, A.C., Appl. Phys. Letters, 17 75 (1970).

32. Gibson, A.F., Kimmitt, M.F., Laser Focus, Aug. (1972).

33. Griem, H.R., Plasma Spectroscopy, McGraw-Hill (1964).

34. Spitzer, L., Physics of Fully Ionized Gases, John Wiley and Sons, 2nd Edition (1962).

35. McWhirter, R.P.W., Plasma Diagnostic Techniques edited by R.H. Huddlestone and S.L. Leonard, (Academic, N.Y., 1965).

36. Crek, B., Pepin, H., Johnson, T.W., Leboeuf, J.N., Nuclear Fusion, 17, 6, (1977).